

NASA TECHNICAL
MEMORANDUM



NASA TM X-3412

NASA TM X-3412

CASE FILE
COPY

FULL-SCALE CRASH TEST
OF A CH-47C HELICOPTER

Claude B. Castle

Langley Research Center

Hampton, Va. 23665



1. Report No. NASA TM X-3412		2. Government Accession No.		3. Recipient's Catalog No.	
4. Title and Subtitle FULL-SCALE CRASH TEST OF A CH-47C HELICOPTER				5. Report Date December 1976	
				6. Performing Organization Code	
7. Author(s) Claude B. Castle				8. Performing Organization Report No. L-10854	
				10. Work Unit No. 505-02-13-01	
9. Performing Organization Name and Address NASA Langley Research Center Hampton, VA 23665				11. Contract or Grant No.	
				13. Type of Report and Period Covered Technical Memorandum	
12. Sponsoring Agency Name and Address National Aeronautics and Space Administration Washington, DC 20546				14. Sponsoring Agency Code	
15. Supplementary Notes Technical Film Supplement L-1211 available on request.					
16. Abstract A full-scale crash test of a large troop/cargo carrying CH-47C helicopter was conducted at the Langley impact dynamics research facility. The crash test of this large helicopter was performed as part of a joint U.S. Army-NASA helicopter test program to provide dynamic structural and seat response data. The purpose of this paper is to report on the test, the procedures employed, the instrumentation, a general assessment of the resulting damage, and typical levels of accelerations experienced during the crash. Various energy-absorbing seating systems for crew and troops were installed and instrumented to provide data for use in the development of design criteria for future aircraft. The crash conditions were selected to simulate known crash conditions and are representative of the 95th-percentile accident environment for an autorotating helicopter. Visual examination of the crashed test specimen indicated irreparable damage to many of the structural components. The highest accelerations were recorded by the accelerometers located on the cabin floor in the aft section of the helicopter, directly above the primary impact location and on the floor of the cockpit above the secondary impact location(s).					
17. Key Words (Suggested by Author(s)) Aircraft crash damage Energy absorbing seats Crash simulation testing Helicopter crash tests			18. Distribution Statement Unclassified - Unlimited Subject Category 03		
19. Security Classif. (of this report) Unclassified	20. Security Classif. (of this page) Unclassified	21. No. of Pages 37	22. Price* \$3.75		

* For sale by the National Technical Information Service, Springfield, Virginia 22161

FULL-SCALE CRASH TEST OF A CH-47C HELICOPTER

Claude B. Castle
Langley Research Center

SUMMARY

A full-scale crash test of a large troop/cargo carrying CH-47C helicopter was conducted at the Langley impact dynamics research facility. The crash test of this large helicopter was performed as part of a joint U.S. Army-NASA helicopter test program to provide dynamic structural and seat response data. The purpose of this paper is to report on the test, the procedures employed, the instrumentation, a general assessment of the resulting damage, and typical levels of accelerations experienced during the crash. Various energy-absorbing seating systems for crew and troops were installed and instrumented to provide data for use in the development of design criteria for future aircraft. The crash conditions were selected to simulate known crash conditions and are representative of the 95th-percentile accident environment for an autorotating helicopter.

Visual examination of the crashed test specimen indicated irreparable damage to many of the structural components. The highest accelerations were recorded by the accelerometers located on the cabin floor in the aft section of the helicopter, directly above the primary impact location and on the floor of the cockpit above the secondary impact location(s).

INTRODUCTION

The Eustis Directorate, U.S. Army Air Mobility R&D Laboratory, has been actively involved for the past several years in the full-scale testing of Army helicopters in a crash environment. Prior to this test, 38 tests had been performed by the U.S. Army to study structural response, crash resistant fuel systems, and energy-absorbing seat designs. On March 6, 1975, the 39th test was conducted at the Langley impact dynamics research facility. The test vehicle, a troop/cargo CH-47C helicopter, was the largest full-scale helicopter tested by the Army to date. The joint U.S. Army and NASA crash test was conducted to provide dynamic response data of the basic structure and the structural components as well as crash data on energy-absorbing troop and crew seats. Two of the eight energy-absorbing seats are discussed. (For a complete analysis of the energy-absorbing seat program, contact the Eustis Directorate, U.S. Army Air Mobility R&D Laboratory.) Various experimental energy-absorbing seating systems were installed and instrumented to provide data for use in the development of design criteria for future aircraft to improve occupant survivability by improving the seat characteristics. The crash conditions were selected to simulate crash conditions which are representative of the 95th-percentile accident environment.

The primary role of NASA in the program was to conduct the crash test and to record a portion of the data. NASA was also responsible for all the data reduction. The role of the Army was to record a portion of the data, to analyze, and to publish the data.

The purpose of this paper is to document the test, the test procedures, the instrumentation employed, and assess generally the resulting damage and levels of accelerations experienced during the crash. A film supplement (L-1211) is available on the CH-47C crash test. (See request card at back of paper.)

TEST FACILITY

The CH-47C helicopter crash test was performed at the Langley impact dynamics research facility shown in figure 1 and described in reference 1. The basic structure of the facility is the gantry which is 73 m (420 ft) high and 122 m (400 ft) long. It is supported by three sets of inclined legs spread 81 m (267 ft) apart at the ground level and 20 m (67 ft) apart at the 66-m (218-ft) level. There are two inclined legs at one end of the gantry for longitudinal support. A movable bridge spans the gantry at the 66-m (218-ft) level and traverses the length of the gantry. A control room and an observation room are located in the building at the base of the gantry. Along the center line of the gantry at ground level is a strip of reinforced concrete 122 m (400 ft) long, 9.1 m (30 ft) wide, and 0.2 m (0.67 ft) thick which is used as the impact surface. The impact surface has a painted 1-m (3.3-ft) grid system for photographic reference.

The systems necessary to meet the helicopter crash test requirements are shown in figure 2. Swing cable pivot point platforms located at the west end of the gantry support the winches, sheaves, and pulley systems for controlling the length of the swing cables. A pullback platform, attached to the underside of the movable carriage, supports a winch, sheave, and pulley system for controlling the length of the pullback cable. The swing and pullback cables attach to the lifting harness which supports the helicopter from ground lift-off to release position during testing. The harness was attached to special helicopter transmission mounting bolts in both the forward and aft ends of the helicopter and to the swing and pullback cables shown in figure 3. The length of the cables in the harness system was designed so that the helicopter would have a 12° nose-up pitch attitude and 0° roll and yaw attitude at impact. The harness also contained a turnbuckle in each of the eight cables for fine adjustment of the pitch, roll, and yaw attitudes.

The cable release system for the helicopter is shown in figure 4. The harness cable attached to the pullback cable contained pyrotechnically operated cable cutters. The cable cutters on the forward pullback harness cables were located adjacent to the rear swing harness cables to prevent cable interference during cable separation. The harness points attached to the swing cables were connected to the helicopter mounting bolts by pyrotechnic release nuts. The pyrotechnic nuts were fired by a lanyard system (fig. 4) adjusted to activate the firing circuit at the desired descent height during the test. The system consisted of a contact switch that was activated by pulling a pin. A 0.16-cm

(0.0625-in.) steel cable was attached to the pin and extended through a sheave system mounted to the gantry at the 45.7-m (150-ft) level. A 2.27-kg (5-lb) mass attached to the end of the cable maintained the cable system taut as the helicopter was being raised and lowered. A stop was attached to the cable and was adjusted to contact a block at the sheave-mounting fixture when the helicopter reached the desired height for swing cable separation.

Two umbilical cables, used for transmitting data from the helicopter to the instrument van and to the control room, entered the helicopter through the two windows (fig. 3). The umbilicals were draped to each side of the helicopter to maintain symmetry and to keep them out of the reaction area of the swing and pullback cable harness during cable separation. Each umbilical contained a 0.76-cm (0.25-in.) steel cable to carry the loads imposed on the umbilicals. The umbilicals remained attached to the helicopter during the test.

External photographic coverage of the crash test was provided by 14 cameras (at locations shown in fig. 2) using film speeds of 24, 400, and 2000 pictures per second. Two of the cameras were located on top of the gantry. Three scanning and three fixed cameras were located at ground level to view the port side of the helicopter. Two cameras were located at each of three other ground locations; forward, starboard, and aft of the helicopter.

TEST SPECIMEN

The test specimen (fig. 5) was a crash-damaged CH-47C helicopter which had been repaired so that the basic structure and the high mass components were representative of a flightworthy aircraft. The vehicle was a twin-turbine engine, tandem rotor helicopter designed for transportation of cargo, troops, and weapons.

When in service, the CH-47C helicopter is powered by two turboshaft engines mounted aft of the fuselage. The engines simultaneously drive two tandem three-bladed counter-rotating rotors through a combining transmission, drive shafting, and reduction transmissions. The forward transmission, the combining transmission, and the drive shaft are in the cabin section and the aft pylon section. Drive shafting from the combining transmission to the forward transmission is housed within a tunnel along the top of the fuselage. Fuel is carried in pods on each side of the fuselage. The helicopter is equipped with four nonretractable landing gear. An entrance door is located at the forward starboard side of the cargo compartment. A hydraulically powered loading ramp is located at the rear of the cargo compartment. The maximum gross mass of the helicopter is 20 865 kg (46 000 lb) and the empty mass is 8674 kg (19 127 lb).

During testing, iron billets were placed beneath floor plates in the forward closet area, and dry sand was used in the aft auxiliary fuel cell pods to obtain a realistic flight mass for this test of 10 145 kg (22 368 lb), and the mass distribution is shown in the table in figure 6. The center of gravity was located at station 337.7. Onboard batteries were used to provide power to the lights, the cameras, and the pyrotechnic devices. The vehicle axes system is shown in figure 7, and the accelerations in the direction of the positive axes are considered positive.

The type and location of the various conceptual energy-absorbing seats are shown in figure 7. All seats were mounted on steel floor plates with the exception of the side-facing troop seat which was mounted directly to the floor structure. Anthropomorphic dummies were placed in nine different seats to measure realistic forces on the seat structure during impact.

To illustrate the type and scope of data recorded, two seat locations on the helicopter were chosen as typical seats and are discussed in this section. The two seat locations (see fig. 7) include one energy-absorbing crew seat at location C and an energy-absorbing troop seat at location F₁. The instrumentation included accelerometers located on the floor, the seat, and in the pelvic region of an anthropomorphic dummy.

The energy-absorbing crew seat shown in figure 8 is essentially a standard armored seat bucket attached to a frame designed to accommodate longitudinal, lateral, and vertical loads simultaneously. The energy-absorbing seat frame consists of a vertical tubular guide rail mounted to the floor through a universal joint which permits the seat frame to rotate in any horizontal direction. The slider (to which the seat bucket is attached and which encompasses the tubular rail) is free to slide up and down. Three torus wire energy absorbers are used to stabilize the seat for normal loads and to limit the loads imposed during a crash situation.

The vertical energy absorber is attached to the tubular rail at one end and the other end is attached to the slider. The longitudinal and lateral energy absorbers are also attached at one end to the tubular rail and to a carriage. The planes of all energy absorbers pass through the center line of the universal joint so that a load in the plane of one axis will not induce loads in an absorber mounted in another axis.

The energy-absorbing troop seat shown in figure 9 consists of a cantilever seat mounted on a truss-type support frame. The seat back and seat pan are constructed of tubular frames covered with fabric. The seat is attached to the ceiling by a compact wire which runs through a roller energy absorber which attenuates the vertical accelerations. The longitudinal accelerations are attenuated by the struts attached to the front of the seat pan through free rotating ball-type attachments. The struts extend diagonally to the free rotating quick-disconnect fitting at the rear of the seat. The energy-absorbing struts for this test consisted of stiff wire connected internally to the ends of the telescoping tubes and bent across a roller. This roller causes the bend to move along the wire as the telescoping tubes stroke. The force required to bend and straighten the wire provides the longitudinal energy absorption for the seat. The lateral accelerations on the seat are attenuated by the steel cables at both the front and the rear of the seat. The steel cables extend diagonally from the seat to the floor.

INSTRUMENTATION

Onboard instrumentation used to obtain data pertaining to the dynamic behavior of the helicopter structure, major components, and various seating

systems included 89 accelerometers, 32 strain gages, 6 deflection indicators, 2 load cells, and 7 high-speed motion-picture cameras. The different types of seats, the arrangement of seats, and the locations of accelerometers are shown in figure 7. The data signals were transmitted through one umbilical to the control room and another umbilical to an instrument van and were recorded on FM tape recorders. To correlate the data signals on the FM recorders and the external motion-picture camera data, a time code from an IRIG-A time code generator was recorded simultaneously on the magnetic tape and on the film. There was also a time code generator onboard the helicopter for the onboard cameras. Typical accelerometer mounts are shown in figure 10. The interior lighting was provided by 70 flash bulbs which were fired in two banks of 35 flashes each. A typical mount of lights with the associated movie cameras is shown in figure 11. To obtain the horizontal velocity of the helicopter at impact, a Doppler radar unit was placed on the impact surface approximately 61 m (200 ft) aft of the impact point, and the signal was recorded on one channel of an FM tape recorder.

TEST PROCEDURE

The preparation of the test specimen included the installation of various types of seats, instrumentation, interior lights, and masses for the proper drop weight and center-of-gravity (c.g.) location. The second sequence of events involved the attachment of the lifting harness, instrumentation installation and checkout, film loading, attachment of the harness to the swing and pullback cables, and checkout and installation of the pyrotechnics. The final sequence was to lift the test specimen to cable separation position, to install the stop on the pyrotechnic firing lanyard, and to lift the specimen to the desired height for subsequent release and the final pendulum swing into the impact area.

With the exception of the firing mechanism of the pyrotechnic devices, the lifting harness (fig. 3) was assembled prior to installation on the test specimen. The instrumentation was connected to the umbilical cables and each channel was checked on an oscilloscope for proper operation. The lifting harness was attached to the two swing cables and the pullback cable. Restraint lines were provided for controlling the motion of these cables after separation. The pyrotechnic firing devices were installed and connected to the release power cable and lanyard firing switch.

The test specimen was lifted by the two swing cables and pullback cable winches until the center of gravity was raised to the proper longitudinal and vertical position (fig. 12). With the test specimen in this position, the distance from the pivot points to the center of gravity along the swing cables was 105 m (344 ft), the radius of the arc which the test specimen would follow in the crash sequence. The tangent of the arc at the impact position was the flight path of -53° . The angle of attack was 65° or a nose-up attitude of 12° . Both still and 16-mm motion pictures were taken of the test specimen in this position for comparison with the actual crash test sequence. The swing cables were locked in this position, and the test specimen was raised by the pullback cable until the center of gravity of the test specimen was at the desired height (fig. 13) of 15.7 m (51.4 ft). This height was calculated to give a flight-path velocity of 15.2 m/sec (50.0 ft/sec) at impact. When the aft landing gear was

raised approximately 0.3 m (1 ft) above the impact surface, the lifting sequence was halted to install the firing lanyard stop which would initiate cable separation during the crash sequence.

The crash test sequence began when the instrumentation recording equipment was started manually approximately 30 sec prior to releasing the test specimen. The release of the test specimen was initiated in the control room by a push switch which closed relays and sent signals from the pyrotechnic power supply to the guillotine cable cutters in the pullback harness. A second and third relay initiated external and internal camera coverage. A lanyard system for the internal flight programmer initiated the light sequence after approximately 1 sec of free fall time. When the test specimen dropped to where the landing gear was approximately 0.3 m (1 ft) above the impact surface, the lanyard was pulled to fire the swing cable harness pyrotechnics, which separated all harness cables from the test specimen and permitted free flight to time of impact. The desired test parameters are given in table I.

TEST RESULTS AND DISCUSSION

A sequence of photographs taken at 0.05-sec intervals showing the free fall, impact, and a portion of the slide out are presented in figure 14. The third photograph in the sequence shows the helicopter in free flight, just prior to contact, after the swing cable harness has been separated from the helicopter. The subsequent downward pitching of the nose after impact causes the forward landing gear to make contact approximately 0.10 sec later (fifth photograph). Nose contact was made 0.25 sec after impact, as shown in the eighth photograph. The remaining sequence of photographs shows the crushing of the nose section and the rebound of the fuselage structure forward of the landing gear.

Structural Test Data

Typical structural accelerometer time histories are shown in figure 15 for two locations near the center line of the floor plates of the helicopter. These locations are representative of structural areas of the helicopter experiencing maximum or near maximum accelerations during impact.

Vertical time histories.— Figure 15(a) shows the vertical accelerations of the accelerometer mounted at station 479 (fig. 7). This trace indicates a maximum acceleration of $-180g$ as the aft section of the helicopter begins to crush and the forward landing gear makes contact. The initial readings of approximately $-10g$ indicate initial ground contact. By the time the aircraft reaches primary impact ($-180g$), the aft landing tires rupture; this tire rupture is followed by the breakaway of the landing-gear support structure. The last portion of the curve shows the accelerations as the helicopter continues to pitch down and indicates approximately $-60g$; the acceleration then decreases to near $0g$ after secondary (nose) impact. The smooth, least-squares fit data (fig. 15(a)), produced from an averaging of the raw data, indicate acceleration readings of approximately 50 percent of the raw data.

Figure 15(b) shows the vertical acceleration data from an accelerometer mounted in the cockpit portion of the helicopter on the floor near the center line at station 82. The accelerations at this point show -20g during the crushing of the aft section (primary impact); then the accelerations increase to a peak of approximately -110g as the nose section slaps into the pavement.

This transmittal of initial force throughout the helicopter decreases as portions of the structure are detached and crushed, thus demonstrating that some of the impact energy is dissipated as the structure deforms. This detachment and crushing of the structure are most evident at the time of highest accelerations in the cockpit area because at this time the aft accelerometer is reading almost 0g. The rebounding, caused by the fulcrum effect at the nose section, continues with several decreasing peaks after the secondary impact has occurred.

Longitudinal time histories.- The longitudinal accelerations in the aft section (fig. 15(c)) were the highest when the aft section fractured at the cabin interface (fig. 14, frame 8). Accelerations of about 40g were recorded.

Lateral time histories.- Figure 15(d) shows the effects of roll and mass distribution as the lateral accelerations oscillate about a positive value rather than zero. The lateral time histories indicate a maximum acceleration of approximately 40g.

Structural Damage and Assessment

The starboard aft landing gear made the first contact with the impact surface. A slight roll was caused by the increased mass on the starboard side as shown by the mass distribution in figure 6. As impact progressed, the aft pylon crushed the aft cabin section and intruded into the aft cabin section approximately 1 m (3.3 ft), as indicated in figure 16. In addition, the relative upward movement of the rear cabin floor in response to the rigid impact surface, coupled with the downward movement of the pylon section, completely closed the aft end of the helicopter (fig. 16(a)). The asymmetrical crushing and starboard list of the vertical sections indicate again the effect of roll and mass asymmetry. Figures 16(b) and 16(c) are closeup photographs of the section at the starboard side and the port side aft landing gear, respectively. It is evident that the impact caused both rear landing-gear tires to rupture and the landing-gear support structure to collapse. The cabin section (fig. 17) was torn by both engines, and these large concentrated masses produced a shearing failure of the aft section of the helicopter. The interior view of the cabin section, looking aft (fig. 16(d)), also indicates the combined effect of a roll attitude and the upward and downward forces applied during impact. The two posts shown are deflection indicators and did not contribute to the structural support of the helicopter: the posts indicated a closure of approximately 0.75 m (29.5 in.) on the starboard side and 0.48 m (18.75 in.) on the port side. The helicopter continued to pitch downward during impact, and the effects of the forward landing gear on the forward cabin section are shown in figure 18. The forward landing gear maintained its integrity (figs. 18(a) and 18(b)) and acted as a fulcrum for the fuselage; this condition caused the floor of the cabin section to be pushed upward as the nose made contact. The relative upward movement of the cabin floor section in the vicinity of the landing gear was approximately 0.68 m (2 ft). An

interior view of this area looking forward in the cabin section is shown in figure 18(c). Again, the two posts shown are deflection indicators and are not a part of the support structure. The posts recorded a closure of the fuselage of approximately 0.23 m (9 in.) on both the starboard and the port side. A view of the same area looking aft (fig. 18(d)) shows the shear separation of the stiffened center floor sections. The pivoting of the nose section about the forward landing gear induced buckling of the bulkheads on both sides of the fuselage (fig. 18(c)) about midway between the floor and ceiling.

The cockpit area shown in figure 19 was not heavily damaged and maintained its livable volume. This lack of damage can be attributed to the crash attitude, and to the large amount of energy dissipated in the crushing of the aft fuselage and in the fuselage section over the forward landing gear. In figures 19(a) and 19(b), a vertical buckle can be seen in the skin over the cabin door, and a longitudinal buckle can be seen at the midpoint of the cockpit. The windshields were removed prior to testing, but both "chin bubble" windows broke on nose contact. The pilot and copilot remained in their seats, but the pilot experienced a downward and forward movement commonly referred to as "submarining" because the pilot did not have a lap belt tiedown strap. The structural deformity (figs. 19(c) and 19(d)) of the floor section beneath the pilot and copilot indicates a clockwise twisting moment. The floor area beneath the copilot is lifted upward while the floor area under the pilot shows that a compressive downward force has been applied.

Representative photographs showing the different types of fuselage damage that occurred during the test are presented in figure 20. The shearing of rivets and the tearing of skin and bulkhead sections of the cabin section in the vicinity of the aft landing gear are shown in figures 20(a) and 20(b). (Black mass in photograph is plastic covering used for weather protection.) Other structural damage can be seen in figure 16(d), where the cabin section has separated; the bulkhead has sheared; and the ceiling plates are bent, torn, and buckled. Figure 20(c) shows the starboard side, looking aft, where the floor plates meet the cabin wall over the forward landing gear. The heavy mounting plate used to hold a bank of lights (fig. 11) remained attached to the floor; however, there was some tearing and bending of this plate due to the relative upward movement of the forward landing gear. Most of the damage in this area occurred under the floor plate and is not evident from the photograph. In spite of this floor damage, all seats remained attached to the primary structure throughout the crash sequence. Figure 20(d) is a view looking aft at the port side where the floor attaches to the sidewall. Here again, most of the major damage occurs near or below the floor area. In this photograph and in figure 18(d), the floor stiffeners are shown to have been sheared by the pivoting action about the forward landing gear.

The onboard motion-picture cameras recorded the initial impact; however, because of the impact, the five cameras inside the cabin did not receive sufficient light for continuing coverage of the crash sequence. The two cameras mounted outside the cockpit (fig. 19(b)) did film the pilot and copilot and did record the complete sequence.

Crew-Seat Test Data

The energy-absorbing crew seat was undamaged during the simulated crash test. However, the telescoping tube torus wire-type vertical absorber failed to function during impact, and the seat did not stroke. A post-tensile test of the absorber revealed that the load required for stroking was, in reality, over two times the preset stroking load. Because of the open-ended tubes, the torus wire-type energy absorbers were susceptible to contamination by environmental factors. In the newer torus wire tubes, efforts have been made to remedy this environmental hazard by coating the inner wall of the tube, by surrounding the wire roller in a viscous fluid, and by sealing the ends of the tube.

Vertical time histories.- Typical accelerometer time histories for the energy-absorbing crew seat are shown in figure 21. Figures 21(a) and 21(b) show data taken from accelerometers mounted on the seat back at approximately the same vertical height (see fig. 10), whereas figure 21(c) shows data taken from the accelerometer mounted on the seat floor plate. The top trace in each figure is a least-squares fit (smooth curve) of the raw data. The second trace shows the smooth curve superimposed on the raw data. The smooth curves (fig. 21) show that the seat accelerometers indicate a reading of -50g on primary impact and approximately -40g on secondary impact. In comparison, the floor accelerometer indicated only -25g on primary impact and -30g on secondary impact.

Longitudinal time histories.- The longitudinal acceleration time histories from the energy-absorbing crew seat and its mounting floor plate are shown in figure 22. The smooth curve for the seat accelerometer indicates an initial acceleration of $\pm 12g$ and $-24g$ for secondary impact. The smooth curve for the floor plate accelerometer indicates a maximum of $\pm 32g$ for primary impact followed by a $\pm 40g$ for secondary impact. The data indicate that the seat received approximately 38 percent of the longitudinal accelerations recorded by the floor plate accelerometer at primary impact and 60 percent at secondary impact. Although there was no stroking of the energy absorbers, the elasticity of the clamping mechanism of the slider to the vertical guide rail did attenuate some of the acceleration input. Therefore, the energy-absorbing crew seat experienced some degree of acceleration attenuation in the longitudinal direction, but not through the designed energy-absorbing mechanism.

Troop-Seat Test Data

Vertical time histories.- The accelerometer time histories from accelerometers located in the pelvic region of the anthropomorphic dummy in the troop seat and on the floor plate beneath the troop seat are shown in figure 23. The location of the troop seat (fig. 7) was such that the impact forces are significant only for the primary impact and not for the secondary impact. The crushing of the helicopter structure dissipated some of the energy between primary and secondary impact, and the accelerometer traces indicate only minute accelerations during secondary impact. These minute accelerations are not considered in the discussion of these traces.

The vertical accelerometer trace in the dummy (fig. 23(a)) indicates a maximum acceleration of -28g for the smooth curve. The smooth curve for the two floor accelerometers (figs. 23(b) and 23(c)) indicates -70g for the accelerometer mounted on the center line of the plate and -80g for the one slightly off the center line. The smooth curve data show that the dummy received about 40 percent of the forces experienced by the floor.

Longitudinal time histories.- The longitudinal time histories for the accelerometers mounted in the dummy and on the troop-seat mounting plate are shown in figure 24. The smooth curve indicates that the dummy had an acceleration of 8g whereas the seat mounting plate had an acceleration of approximately -24g. The traces show that there was a reduction of acceleration of 66 percent between the floor plate and the dummy for the longitudinal accelerations.

Lateral time histories.- The lateral forces, shown in figure 25, indicate an increase of 33 percent in the dummy lateral accelerations over the accelerations of the floor plate. The smooth curves show $\pm 40g$ in the dummy and $\pm 30g$ in the floor plate. The lateral traces indicate that no lateral acceleration attenuation occurs in the seat as the seat is deflected vertically and longitudinally.

CONCLUSIONS

A CH-47C helicopter was successfully crash tested at the Langley impact dynamics research facility. The impact velocities (12.19 m/sec (40.0 ft/sec) vertical, 9.14 m/sec (30 ft/sec) horizontal, and 15.24 m/sec (50 ft/sec) flight path) simulated actual crash conditions and were representative of the 95th-percentile accident environment. Photographic coverage of the crash test was provided by 14 external cameras and 7 internal cameras. Onboard instrumentation included 89 accelerometers, 32 strain gages, 6 extensometers, and 2 load cells. All data signals were recorded on tape and appear to be well defined through secondary impact. There were failures in two external cameras covering the starboard side of the helicopter. Some conclusions reached from the test results are:

1. Visual observation of the helicopter after crash testing indicates severe structural damage in the form of buckling, tearing, and shearing of the cabin structure. Because the rear exit was closed when the engines penetrated the cabin area, personnel could not leave by the rear exit.
2. The highest accelerations on the structure occurred at primary impact and were recorded by the accelerometers located on the aft portion of the cabin floor directly above the point of impact. These accelerations measured 180g vertical, 40g longitudinal, and 40g lateral and lasted about 10 msec.
3. The pitch rotation of the helicopter and subsequent secondary impact of the cockpit produced accelerations in the cockpit as high as 70 percent of the primary structure accelerations.
4. All seats remained attached to the primary structure throughout the crash sequence.

5. There was no acceleration attenuation in the vertical direction for the experimental energy-absorbing crew seat.

6. The crew seat did attenuate some of the floor accelerations in the longitudinal direction because the seat leg clamping mechanism yielded.

7. The design of the energy-absorbing troop seat shows good acceleration attenuation in the vertical and longitudinal direction.

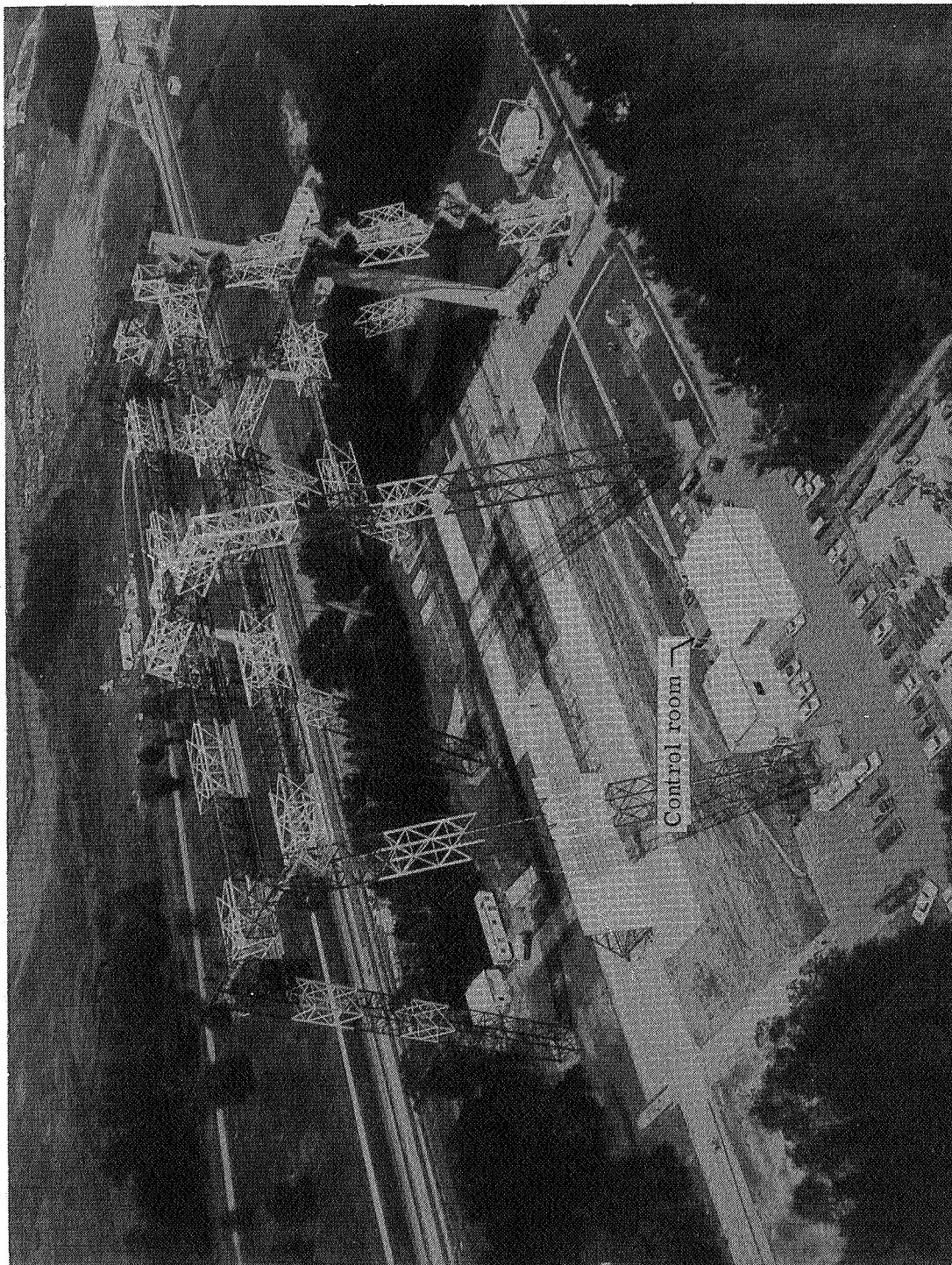
Langley Research Center
National Aeronautics and Space Administration
Hampton, VA 23665
October 4, 1976

REFERENCE

1. Vaughan, Victor L., Jr.; and Alfaro-Bou, Emilio: Impact Dynamics Research Facility for Full-Scale Aircraft Crash Testing. NASA TN D-8179, 1976.

TABLE I.- CRASH TEST PARAMETERS

Test parameter	Planned	Actual
Flight path, deg	-53.0	-53.0
Free flight time, sec	0.02	0.02
Angle of attack, deg	65	63
Pitch angle, deg	12	10
Yaw angle, deg	0.0	0.0
Roll angle, deg	0.0	1.0
Flight-path velocity, m/sec (ft/sec)	15.2 (50.0)	15.0 (49.4)
Vertical velocity, m/sec (ft/sec)	12.2 (40.0)	12.0 (39.4)
Horizontal velocity, m/sec (ft/sec)	9.1 (30.0)	9.1 (29.7)



L-74-2505.2

Figure 1.- Langley impact dynamics research facility.

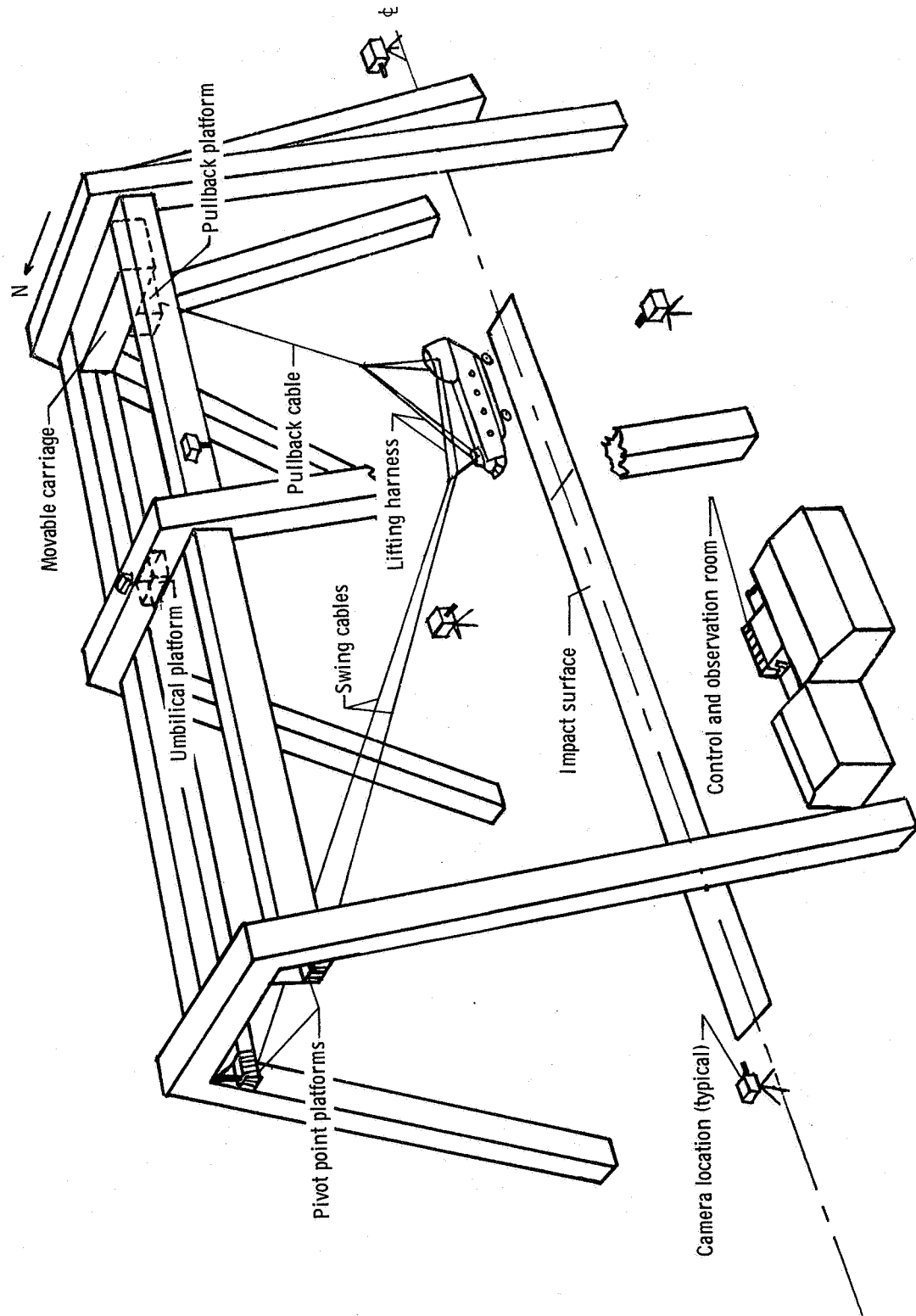


Figure 2.- System used in full-scale crash simulation test.

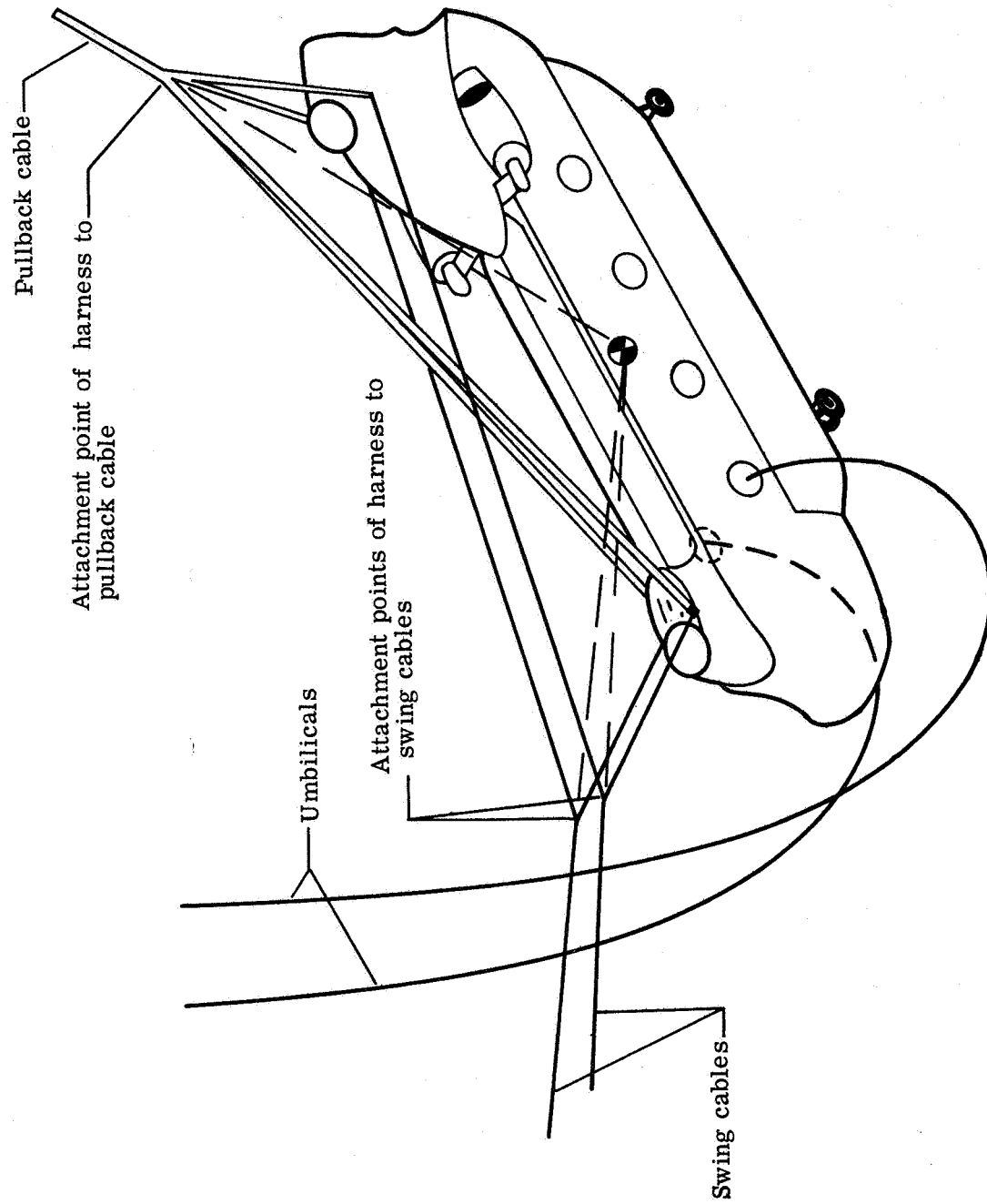


Figure 3.- Lifting harness for test specimen.

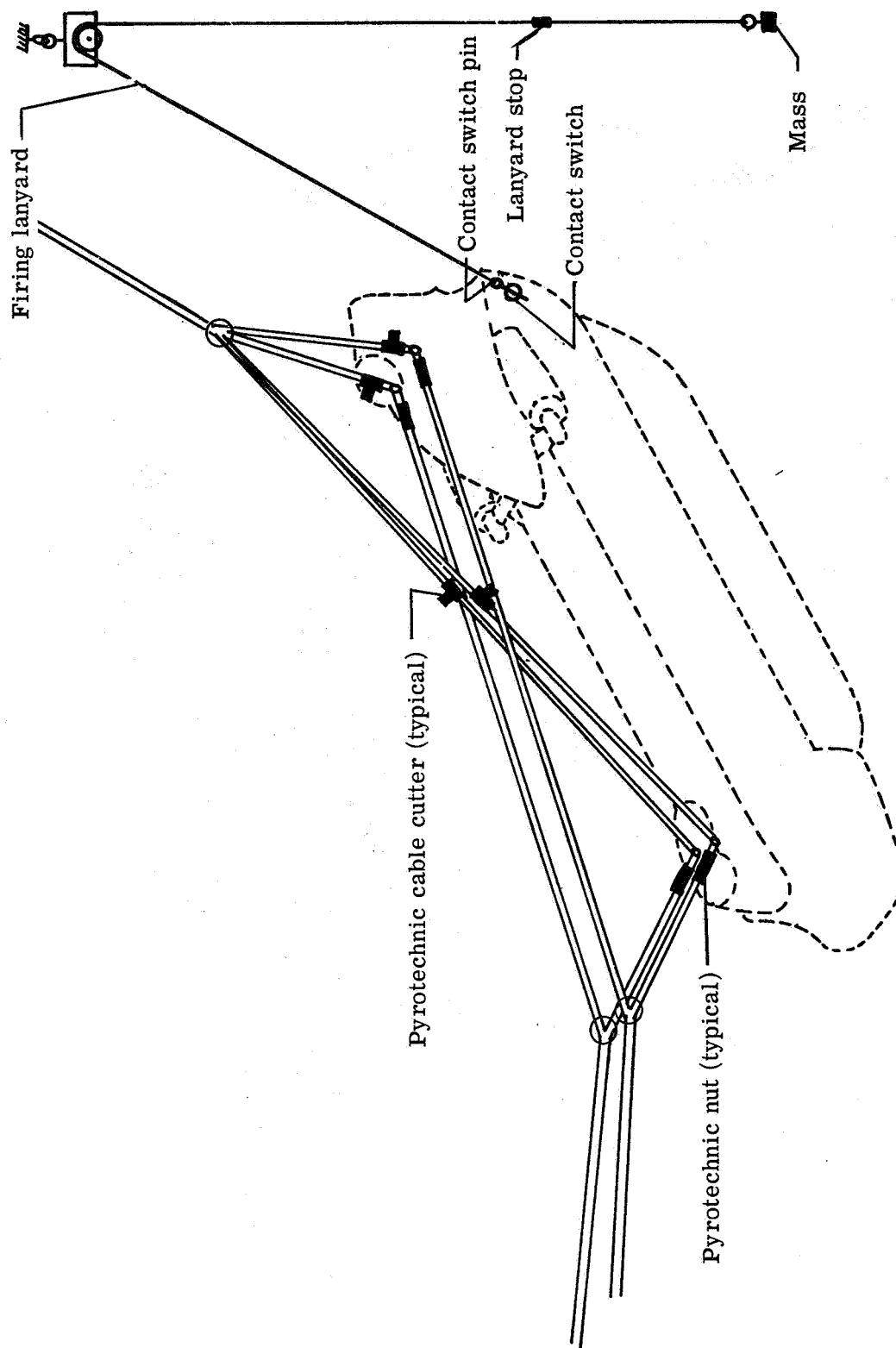
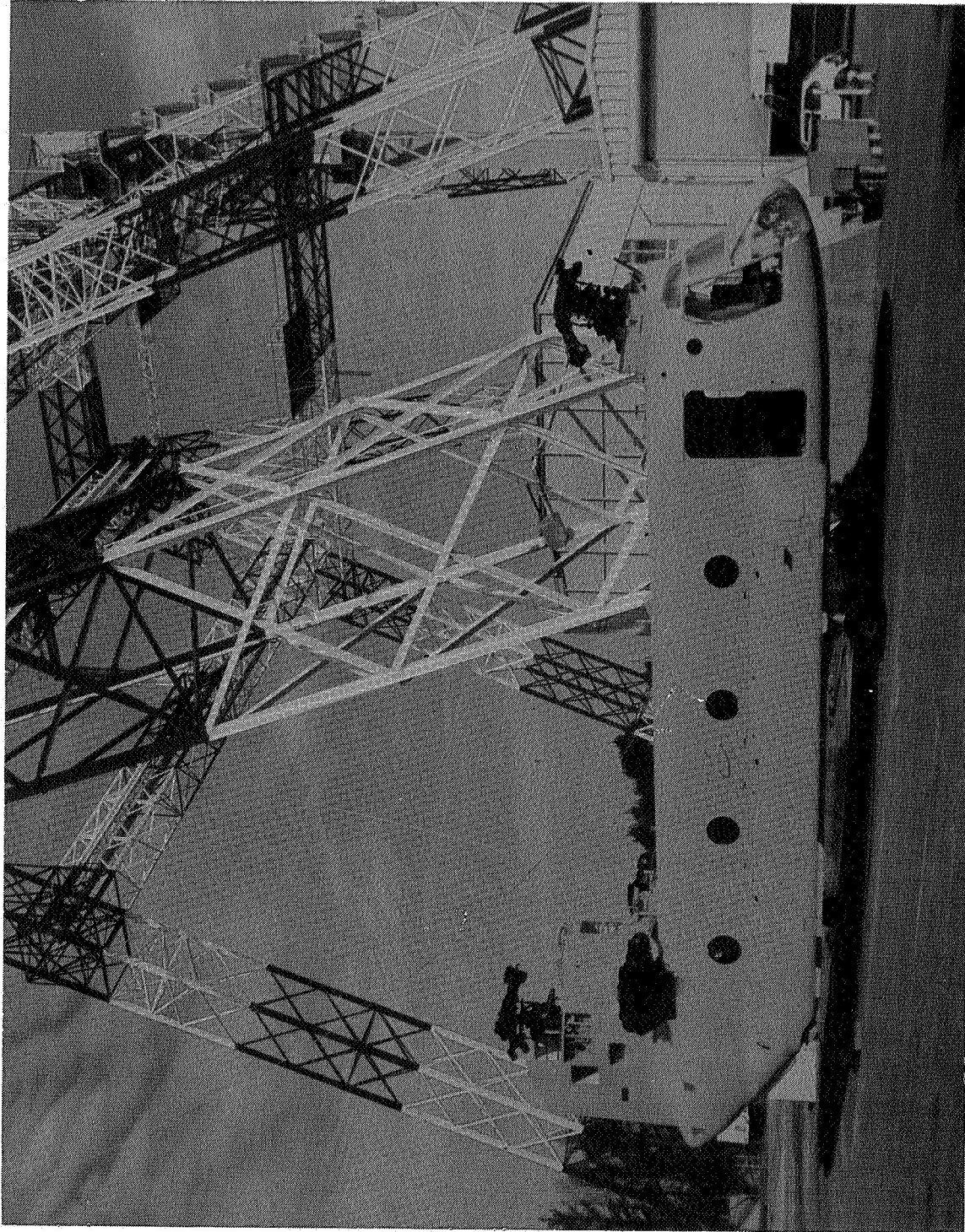


Figure 4.- Cable release system.



L-76-265

Figure 5.- CH-74C helicopter test specimen.

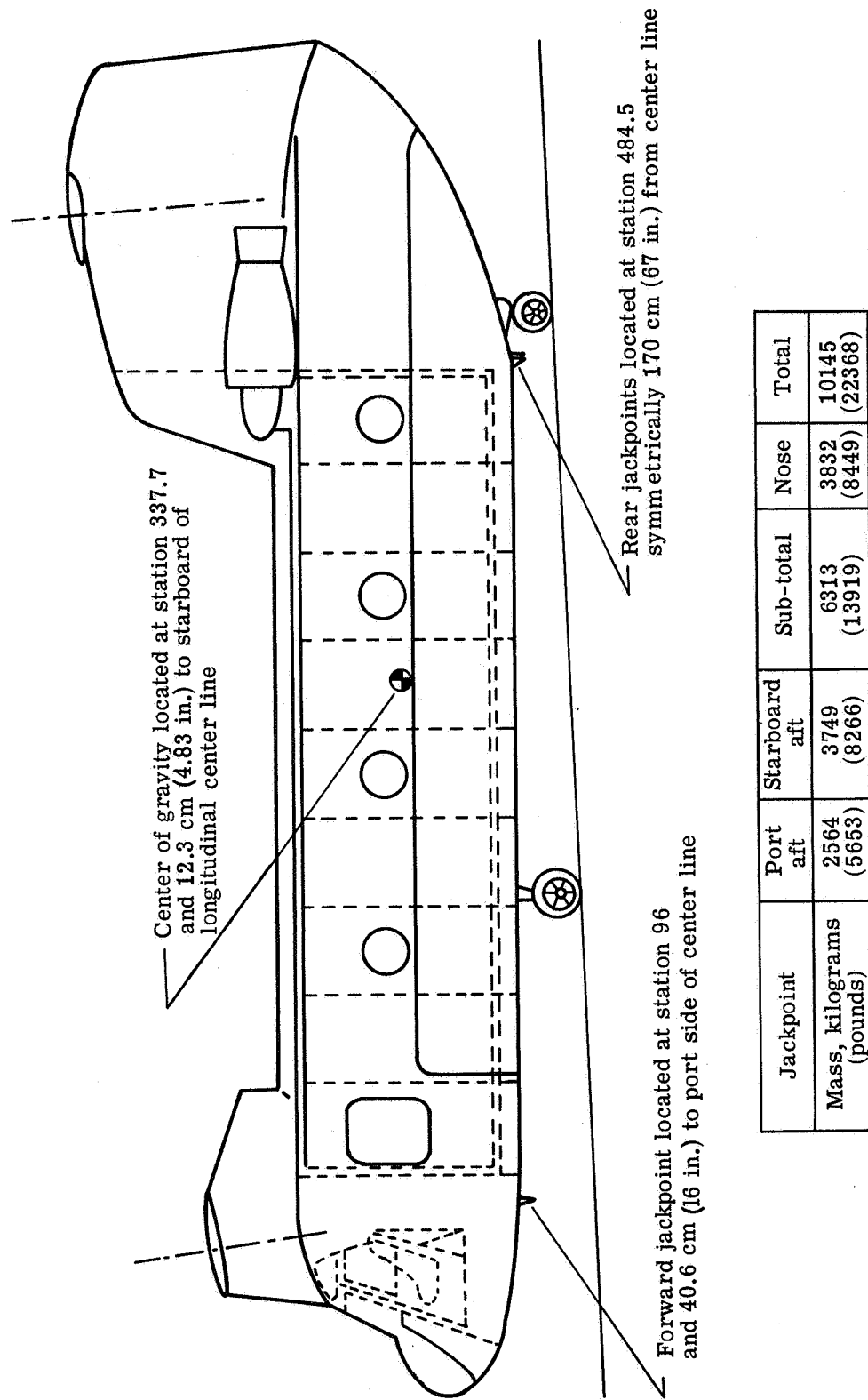
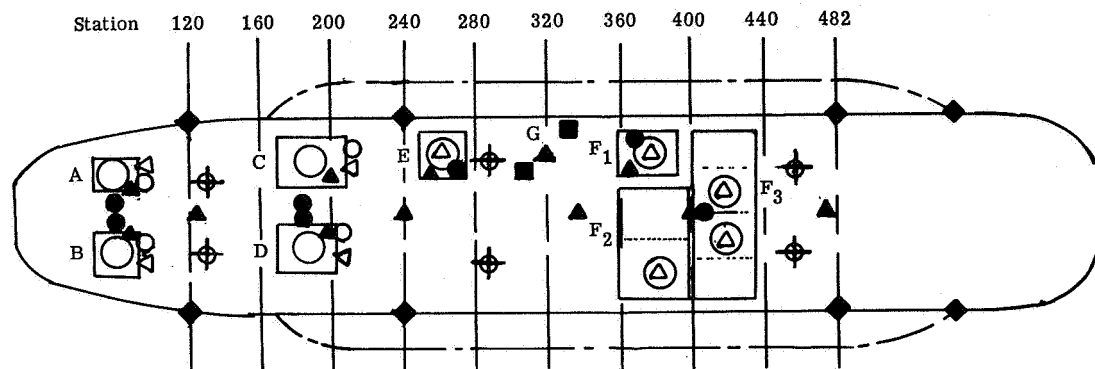












Figure 6.- Mass distribution for test specimen.



Location	A	B-C-D	E	F	G
	Standard unarmored crew seat	Experimental armored crew seat	Experimental side facing troop seat	Experimental troop seat package	Cargo tiedown crash loads

-  Experimental seat locations
-  Experimental seats with dummy
-  Triaxial accelerometer in dummy
-  Triaxial accelerometer on structure
-  Triaxial accelerometer on seat
-  Vertical accelerometer on floor
-  Vertical accelerometer on seat
-  Deflection indicator
-  Strain gage
-  Load cell

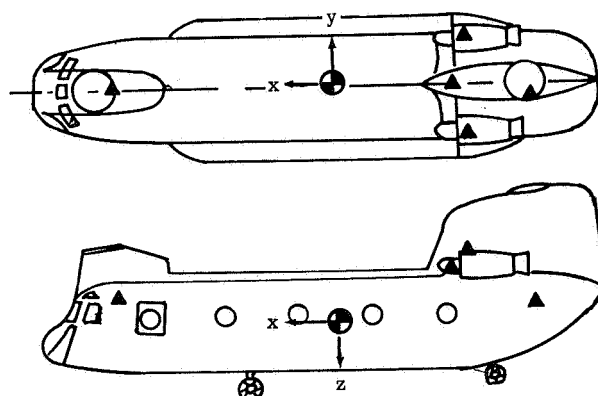
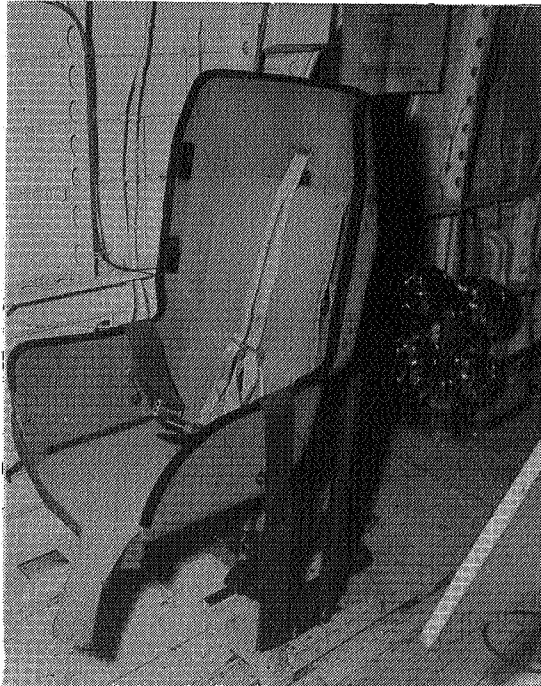
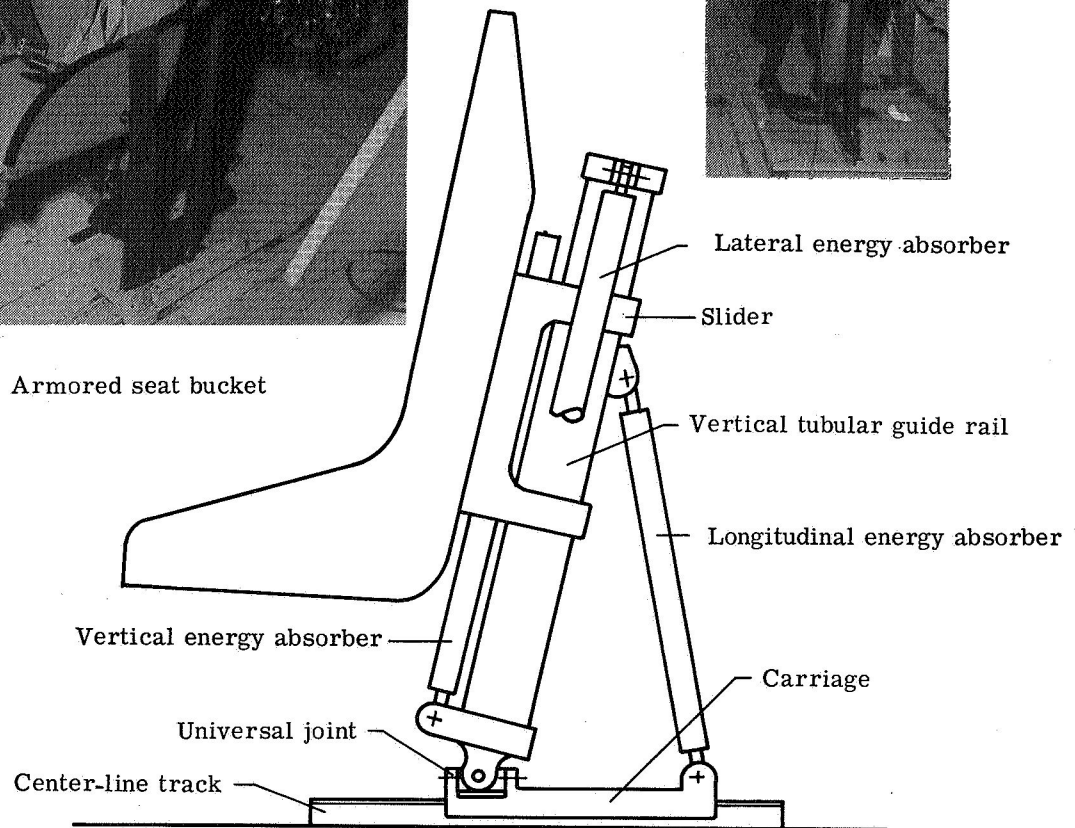


Figure 7.- Interior seat and accelerometer layout.

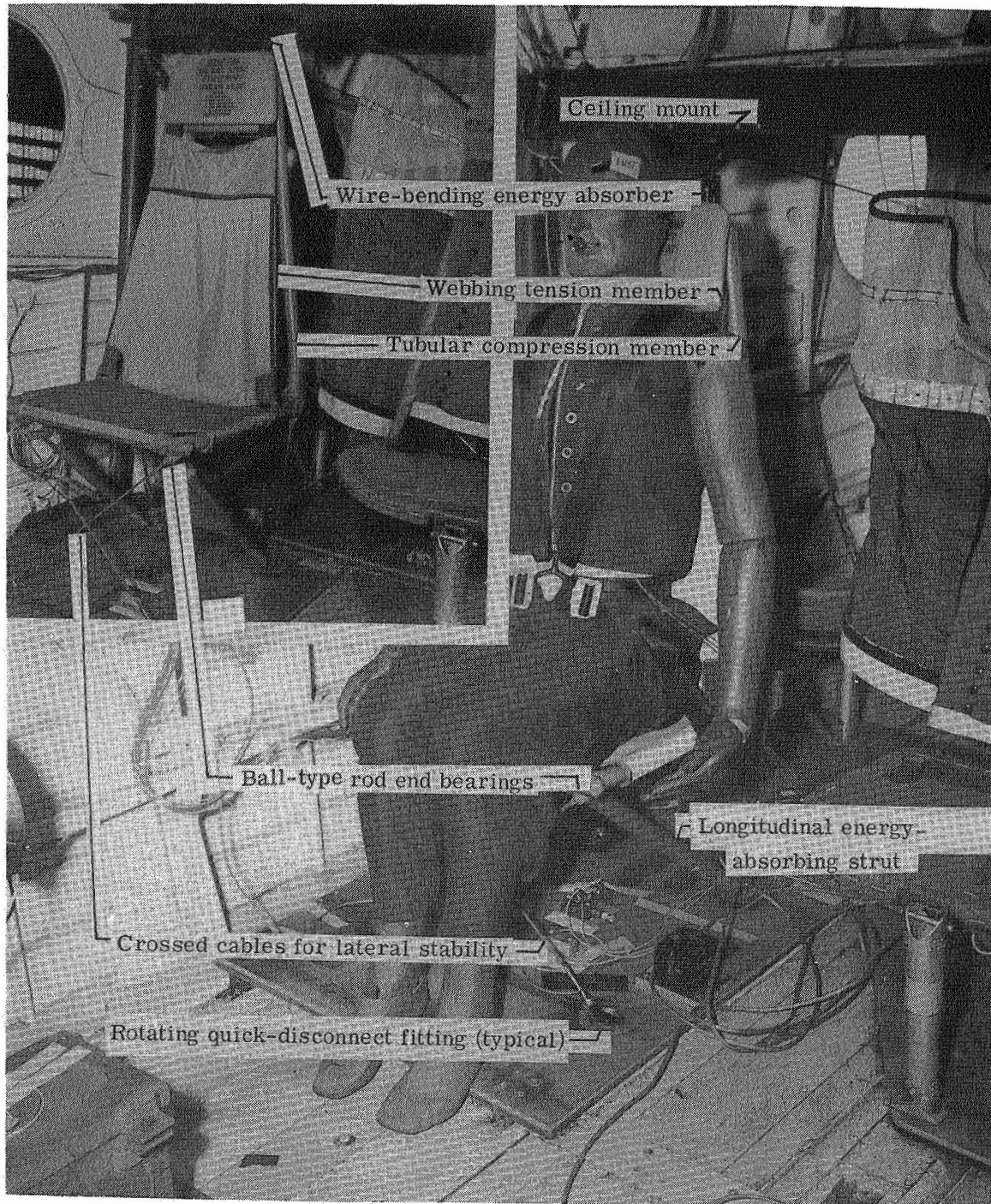


Armored seat bucket



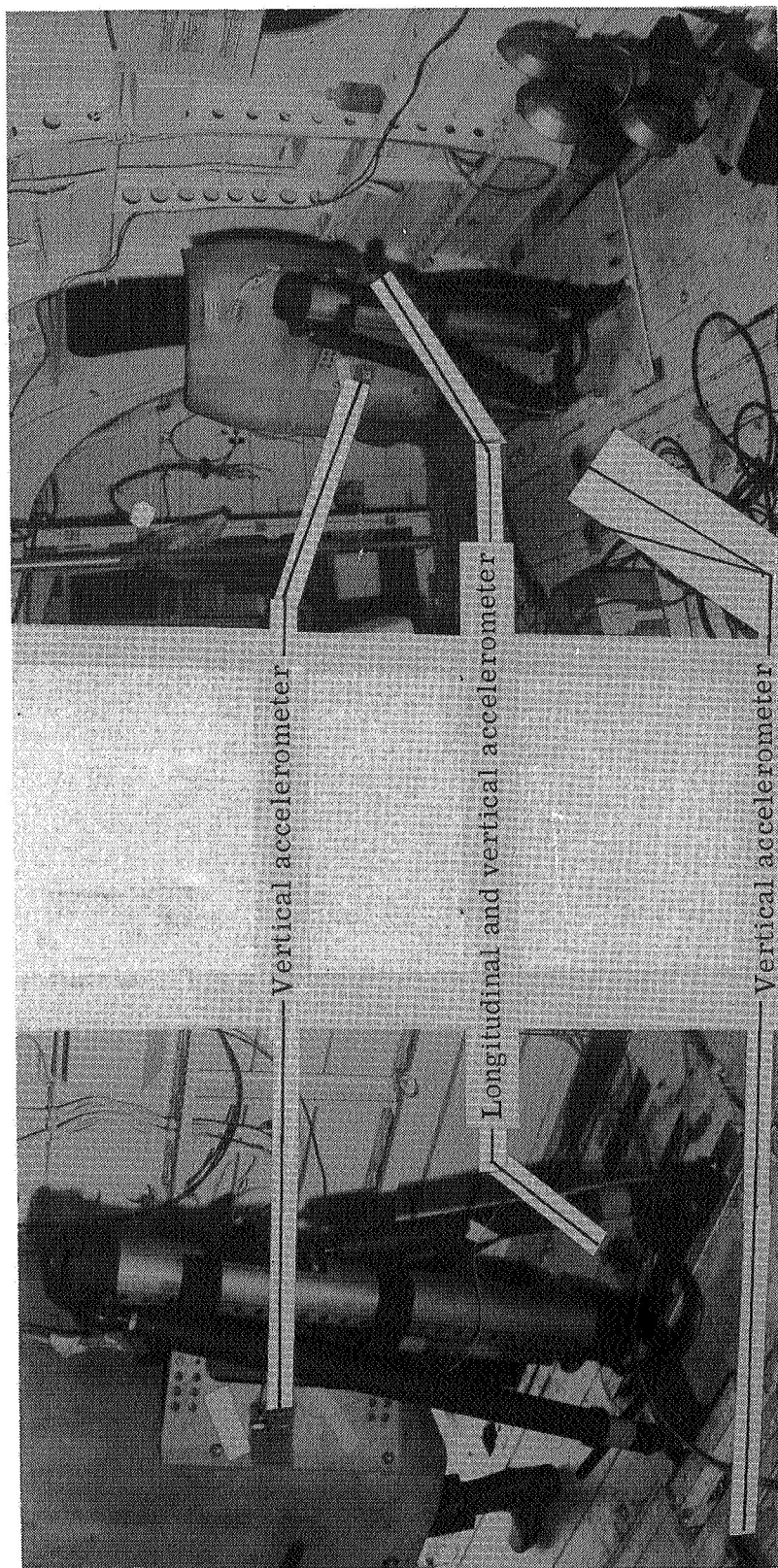
L-76-266

Figure 8.- Energy-absorbing crew seat in location C.



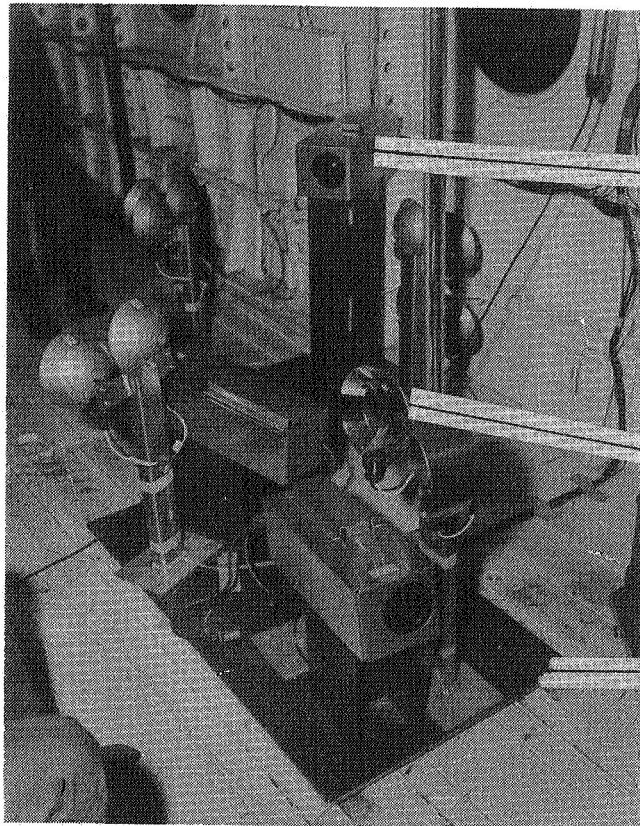
L-76-267

Figure 9.- Energy-absorbing troop seat in location F₁.



L-76-268

Figure 10.- Typical accelerometer mounts and locations.



— Motion-picture camera

— Flash bulb holders and reflectors

— Mounting plate

L-76-269

Figure 11.- Interior motion picture and lighting system.

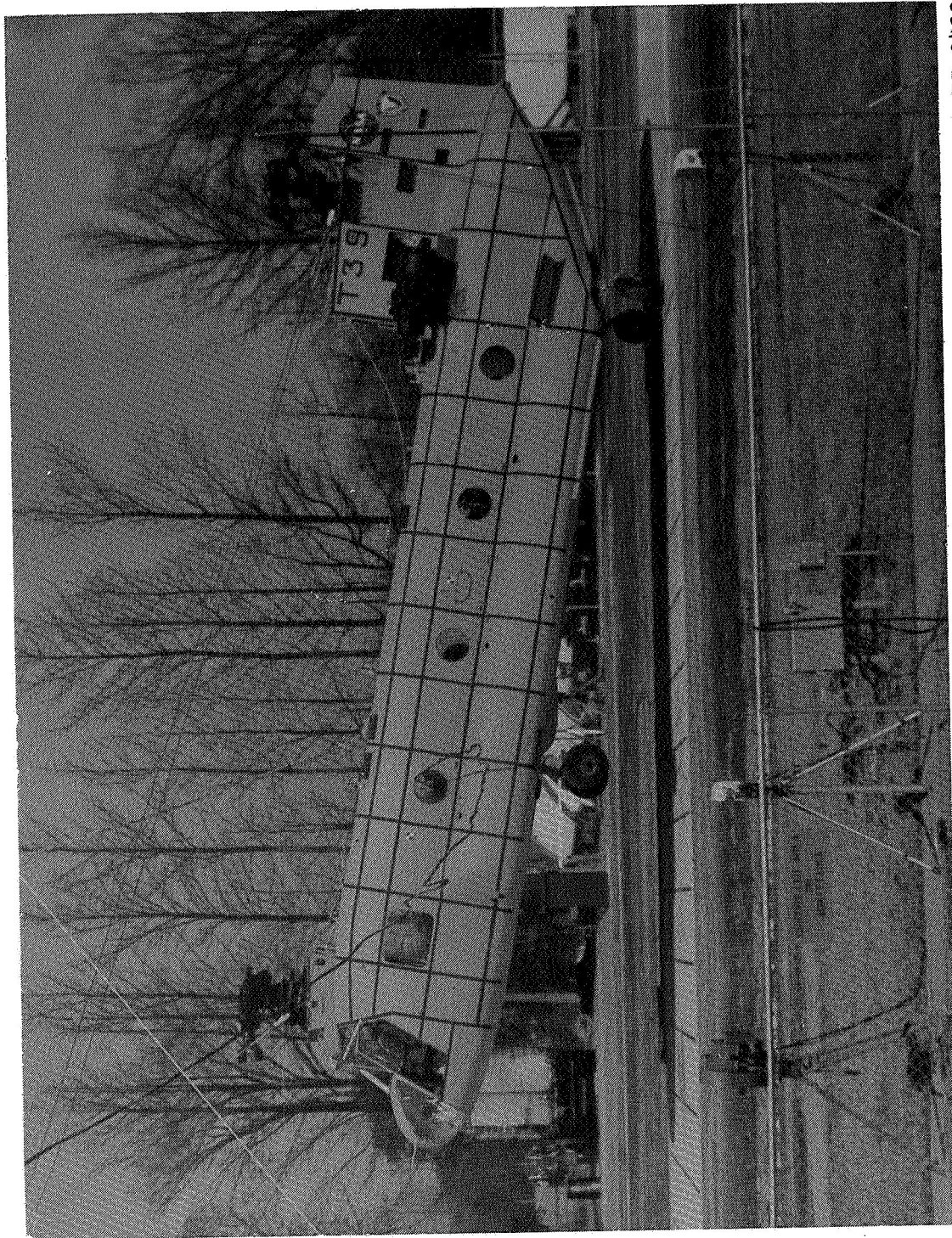
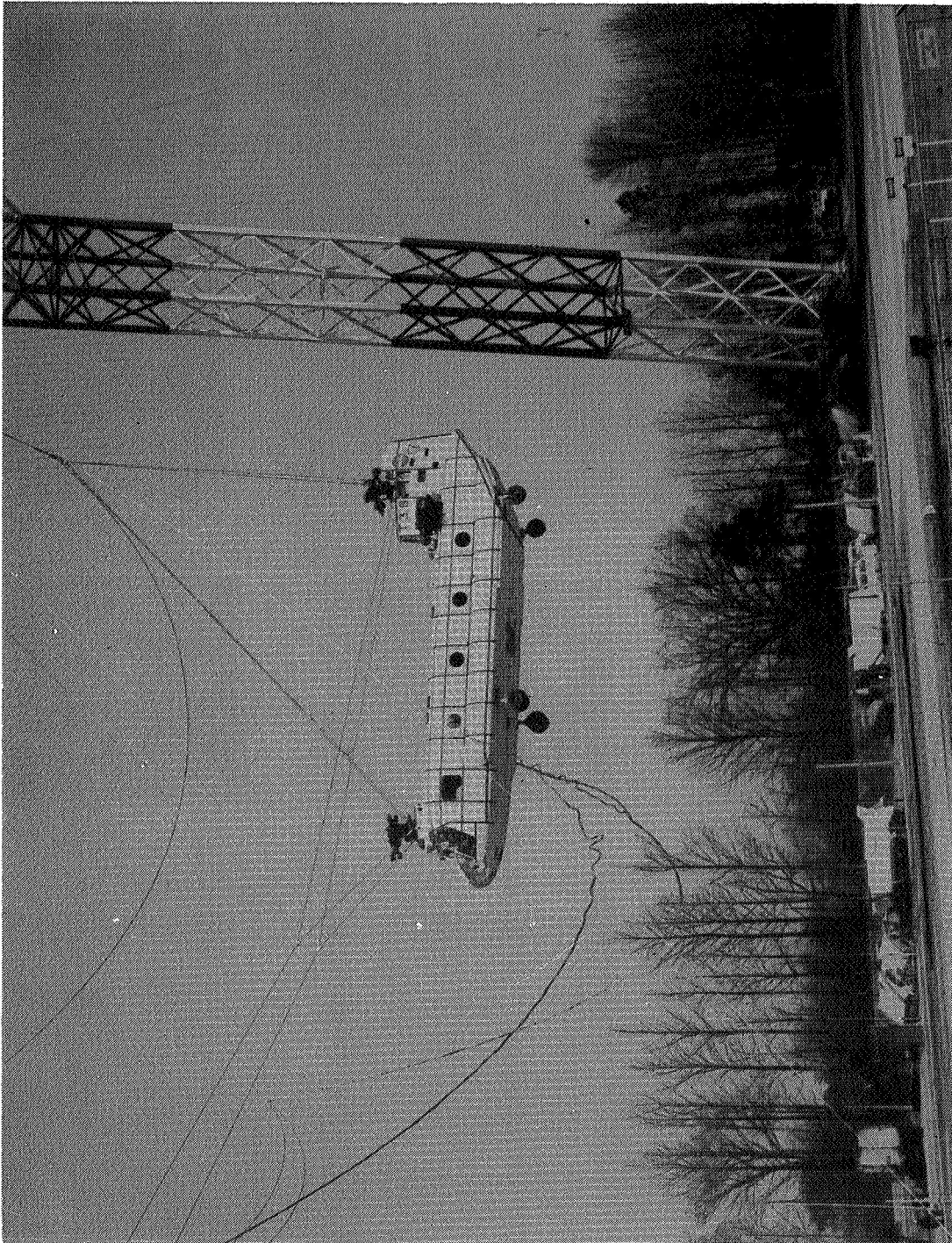


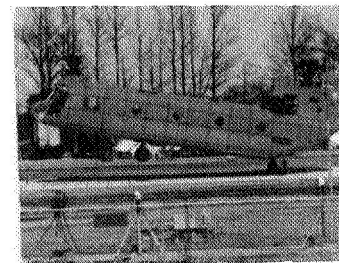
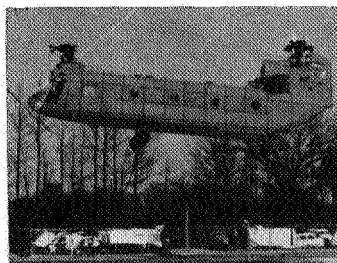
Figure 12.- Test specimen in impact position.

L-75-2432



L-75-1879

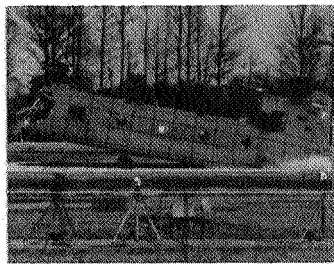
Figure 13.- Test specimen in release position.



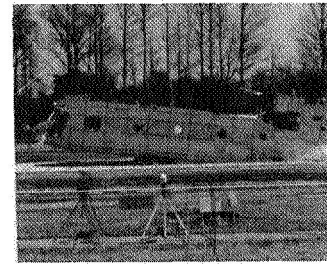
$t = 0.00 \text{ sec}$



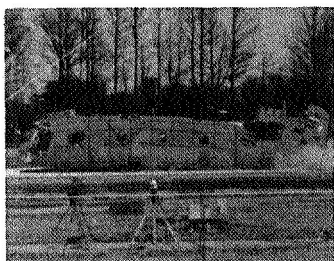
$t = 0.05 \text{ sec}$



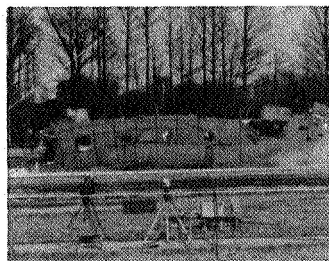
$t = 0.10 \text{ sec}$



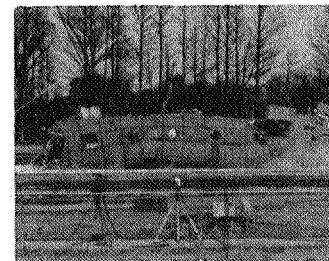
$t = 0.15 \text{ sec}$



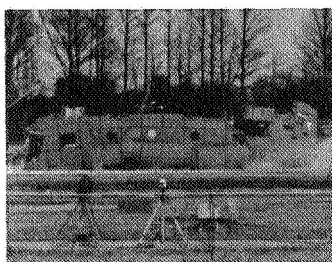
$t = 0.20 \text{ sec}$



$t = 0.25 \text{ sec}$



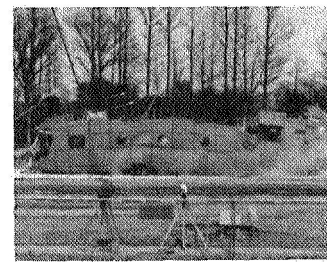
$t = 0.30 \text{ sec}$



$t = 0.35 \text{ sec}$

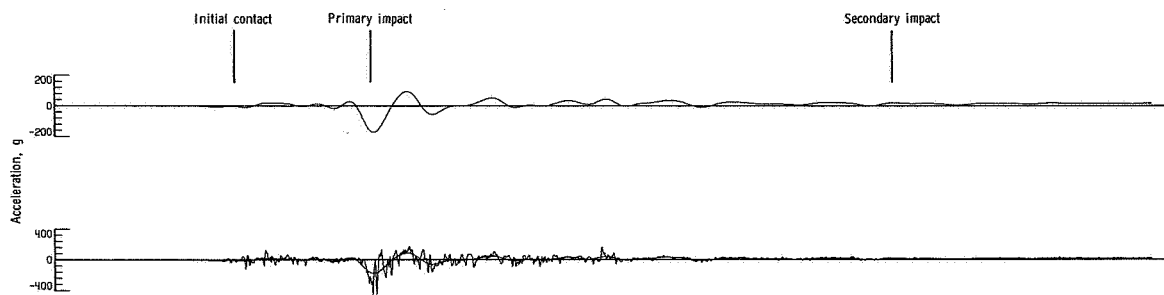


$t = 0.40 \text{ sec}$

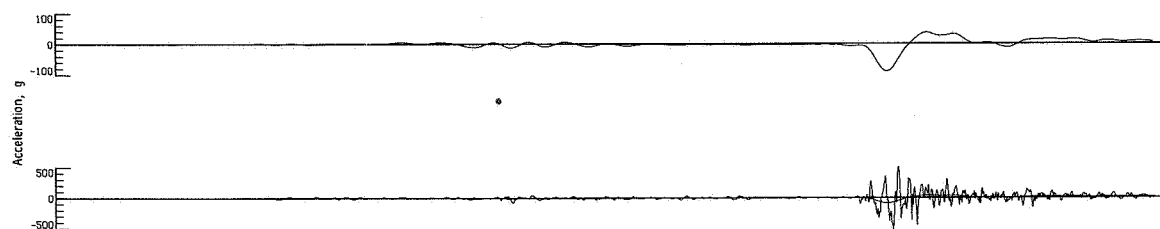


$t = 0.45 \text{ sec}$

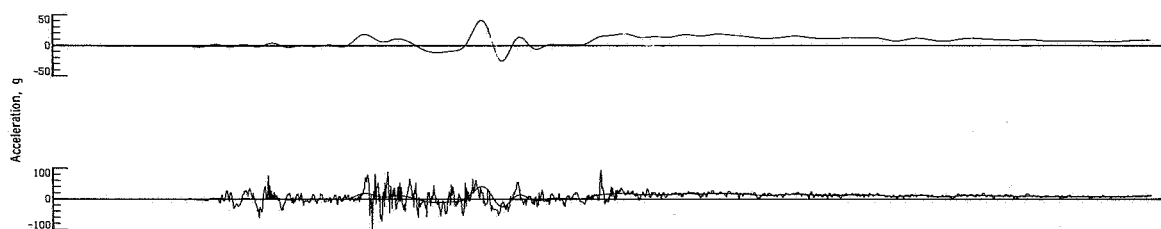
Figure 14.- Sequence of photographs taken at 0.05-sec intervals during testing. L-75-2686.1



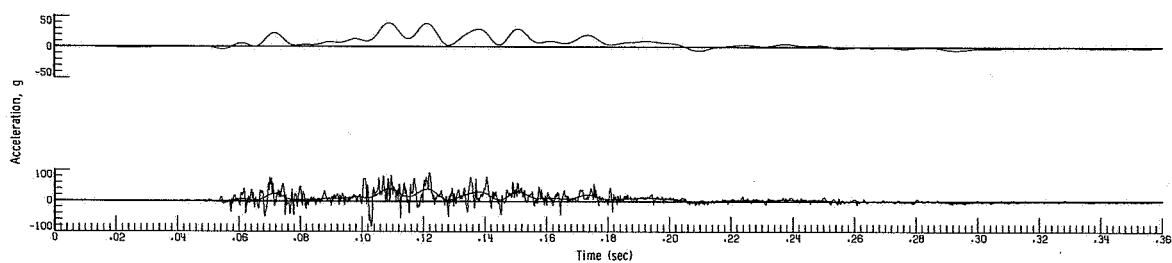
(a) Vertical accelerations at station 479.



(b) Vertical accelerations at station 82.

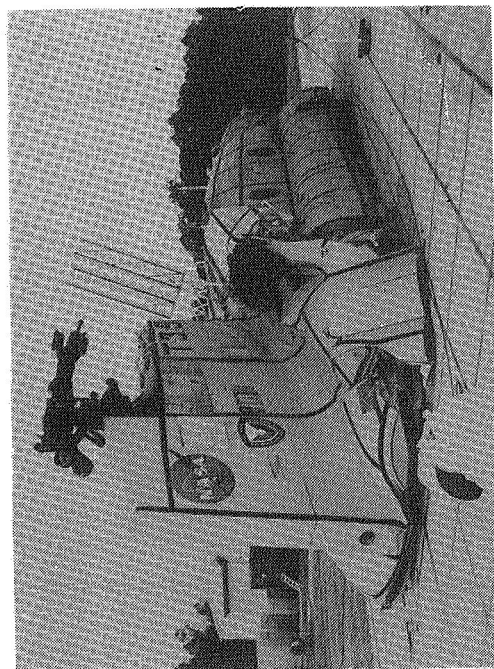


(c) Longitudinal accelerations at station 479.

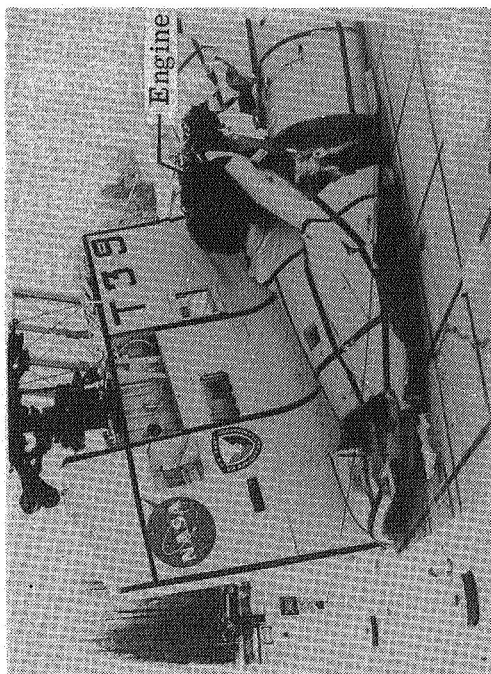


(d) Lateral accelerations at station 479.

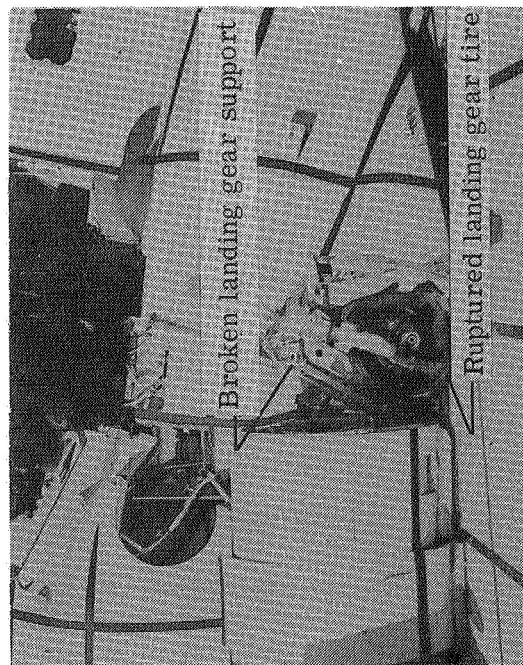
Figure 15.- Structural acceleration time histories for accelerometers mounted on cabin floor at stations 479 and 82.



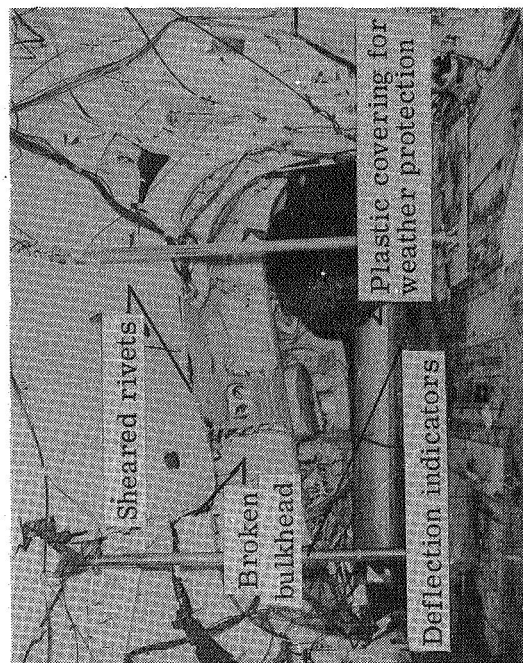
(a) View from rear.



(b) View from starboard side.

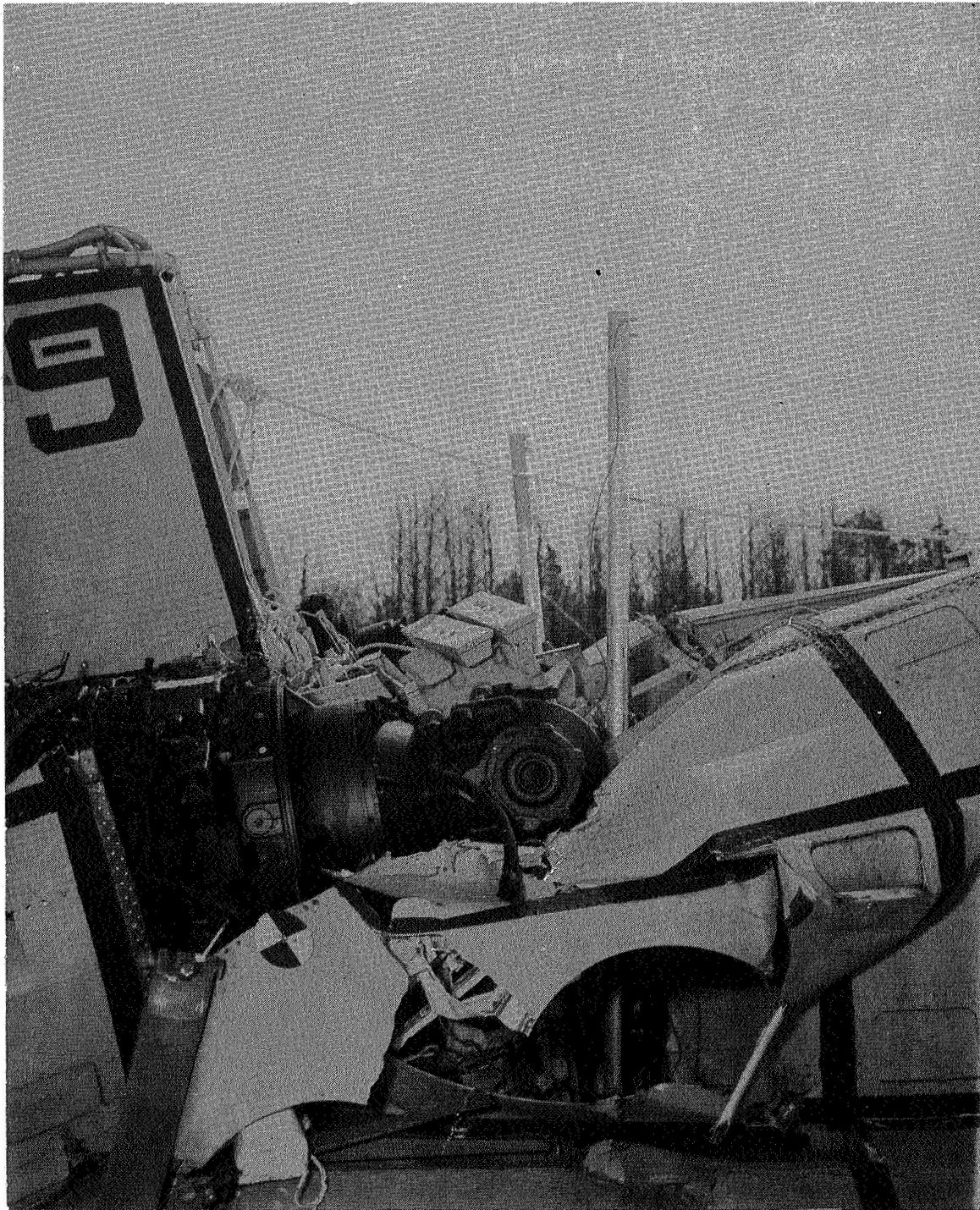


(c) View from port side.



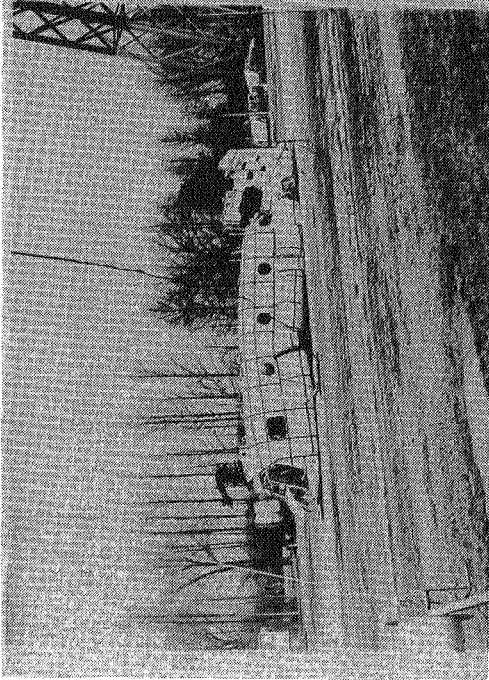
(d) View from inside looking aft.
L-76-270

Figure 16.- Effects of high mass concentrations in impact situations.

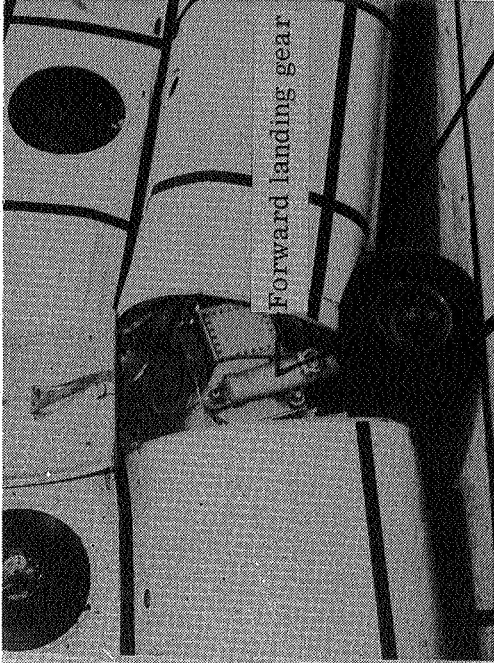


L-76-271

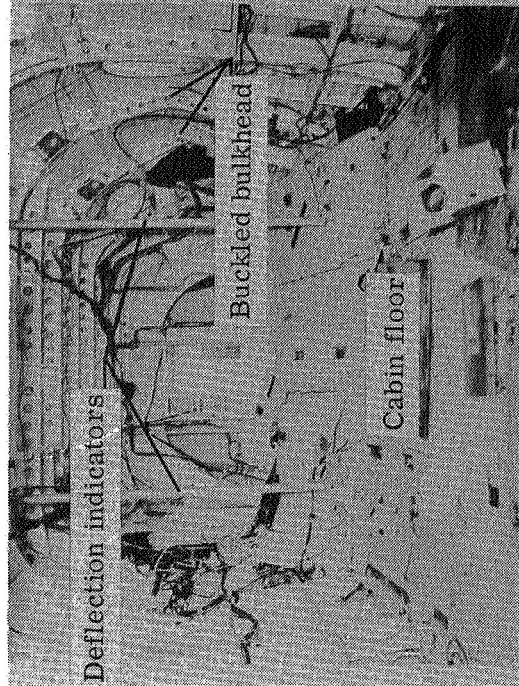
Figure 17.- Effect of large concentrated mass during impact.



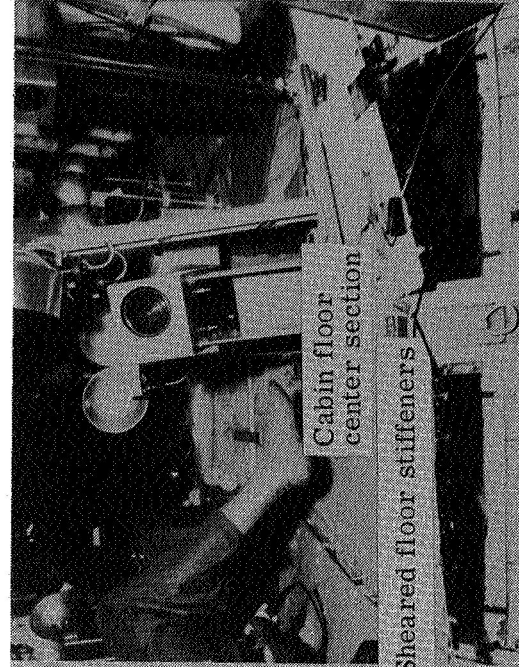
(a) View from port side.



(b) Closeup from port side.

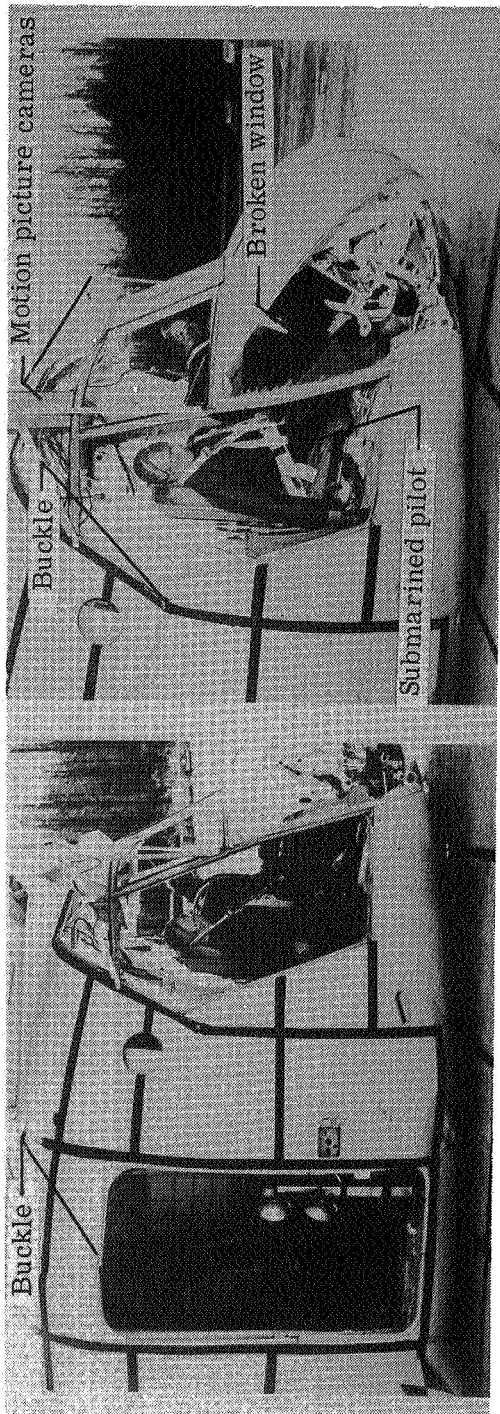


(c) View from inside looking forward.



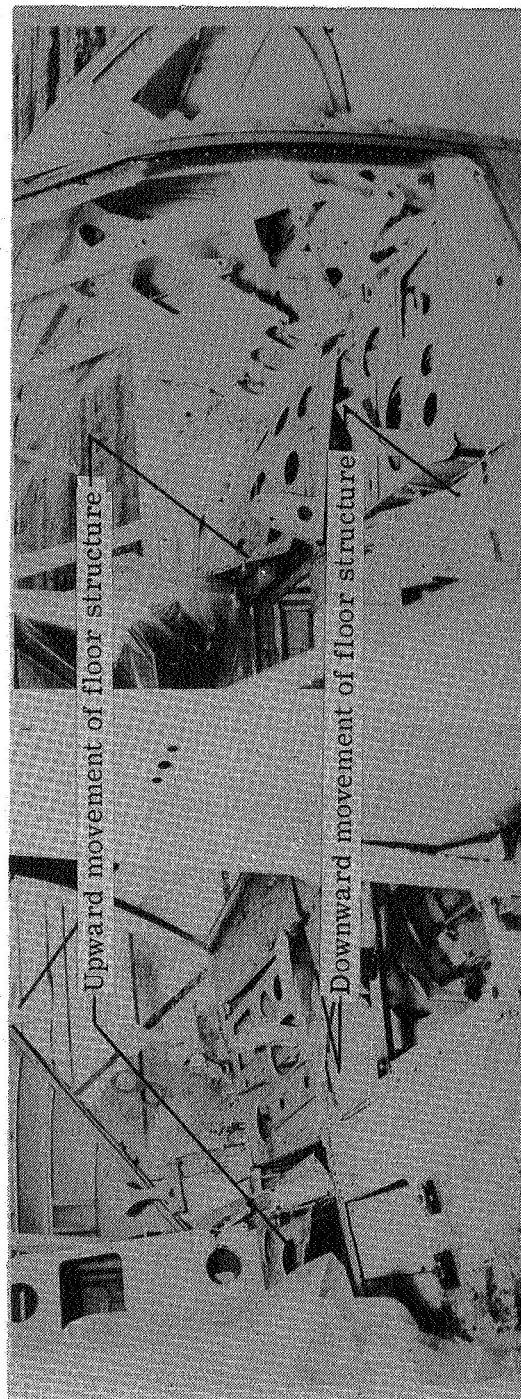
(d) View from inside looking aft.
L-76-272

Figure 18.- Effect of forward landing gear after impact.



(a) View from starboard side.

(b) Closeup from starboard side.

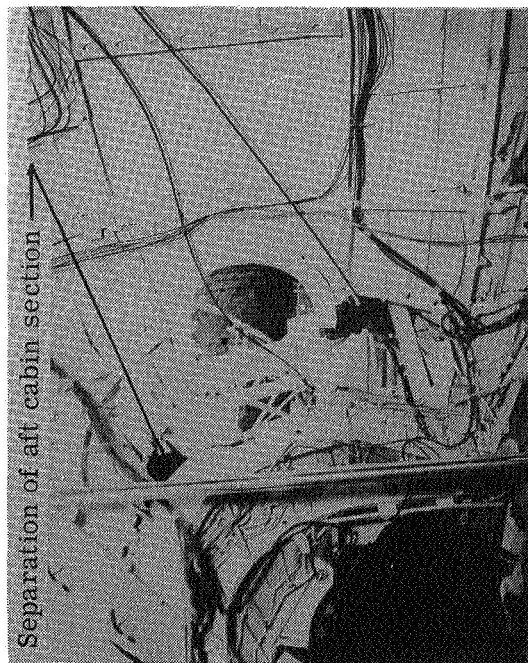


(c) Interior view looking forward.

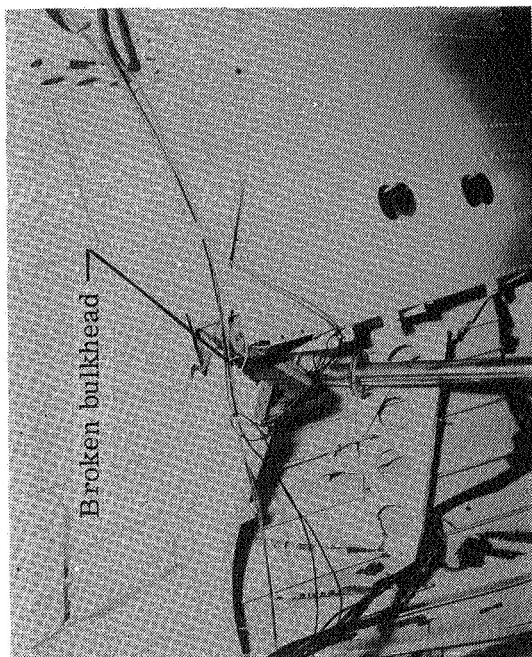
(d) View of interior from starboard side.

Figure 19.- Effects of crash on cockpit section.

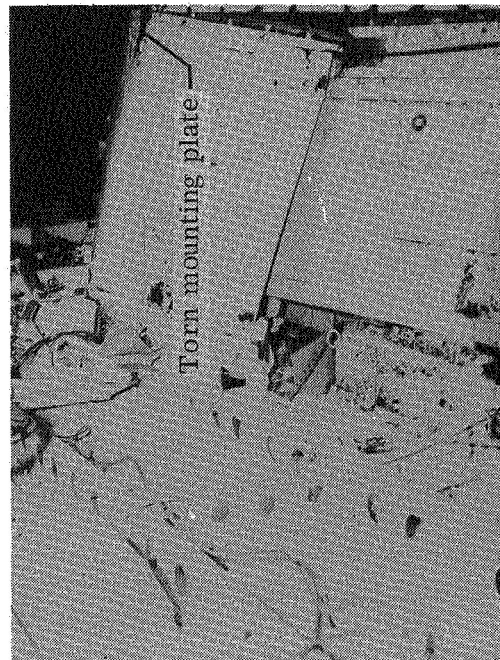
L-76-273



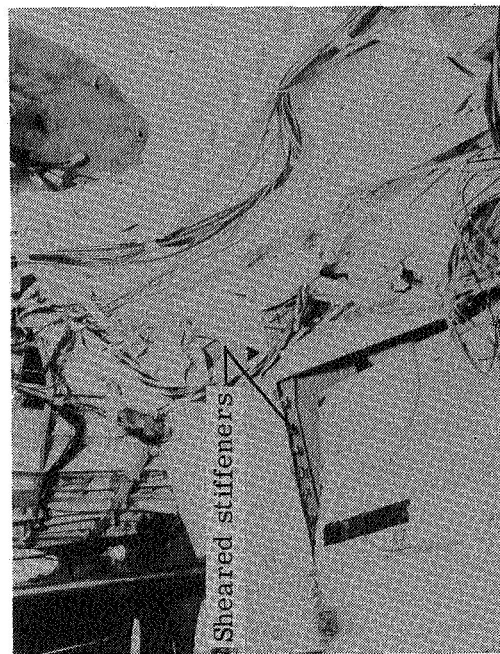
(a) Port side aft section.



(b) Aft roof section.



(c) Starboard side over forward landing gear.



(d) Port side over forward landing gear.
L-76-274

Figure 20.- Typical interior damage scenes of crashed test specimen looking aft.

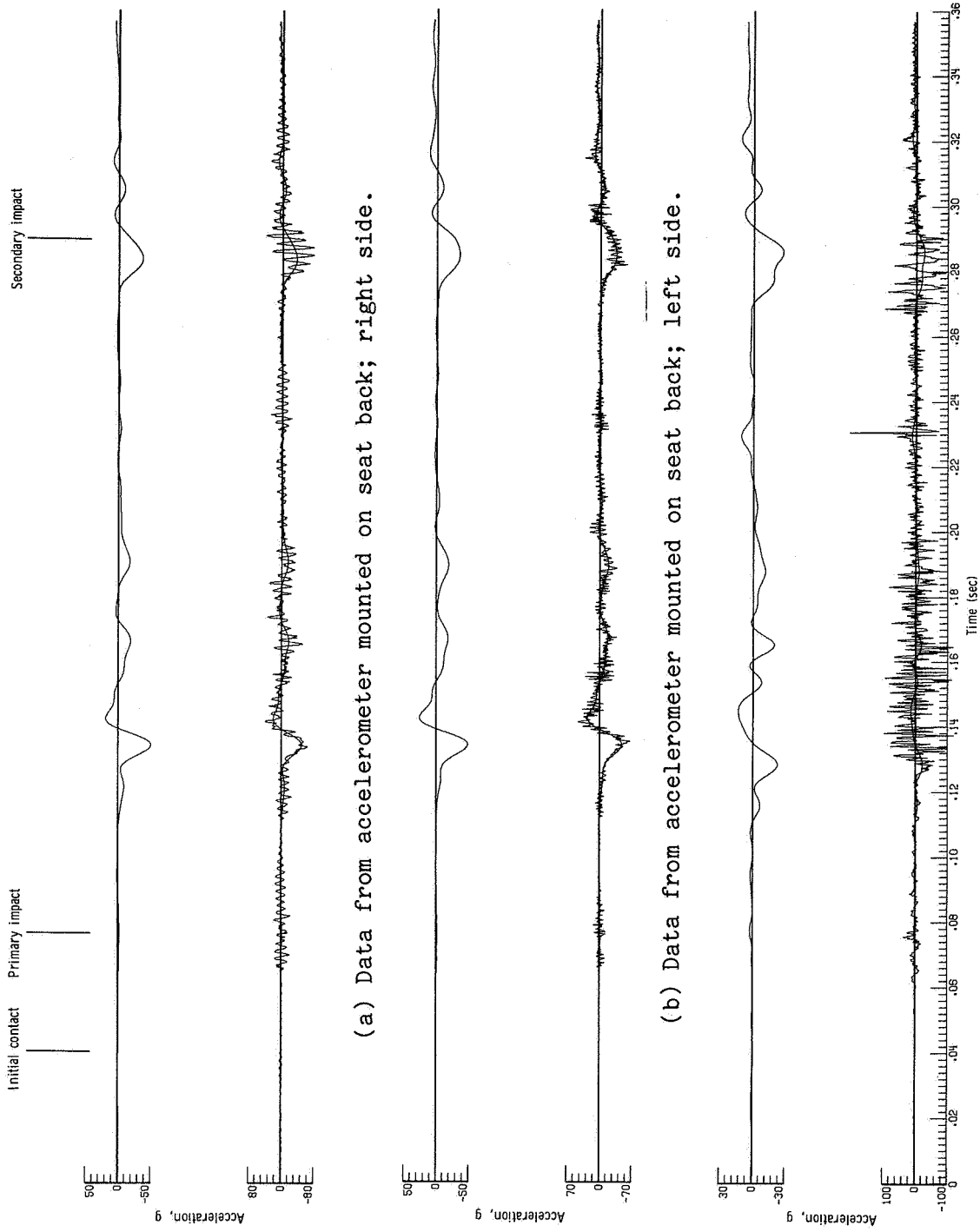
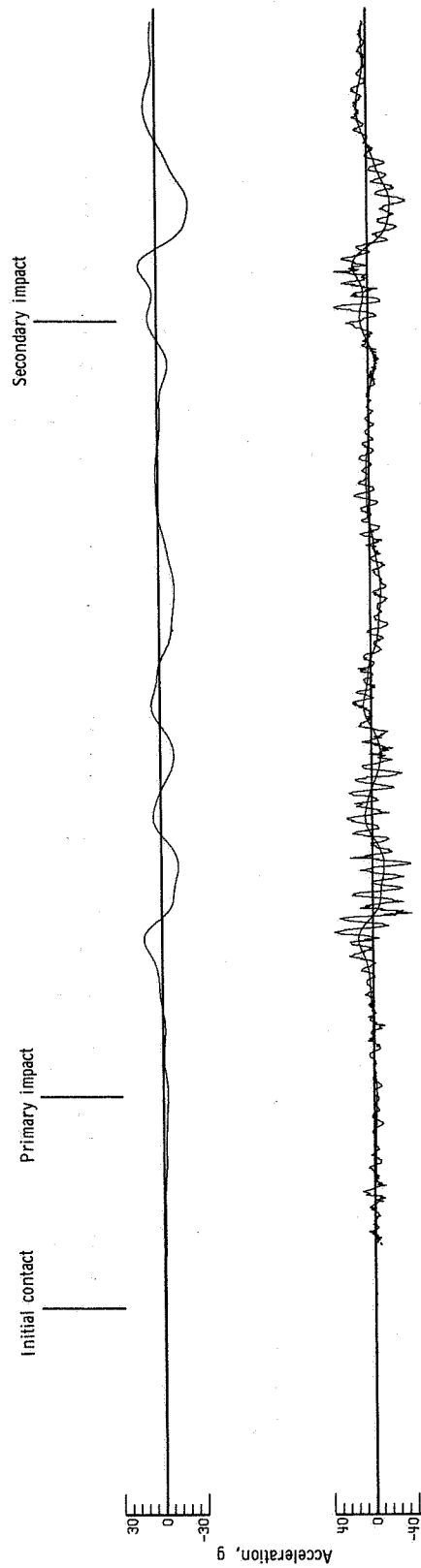
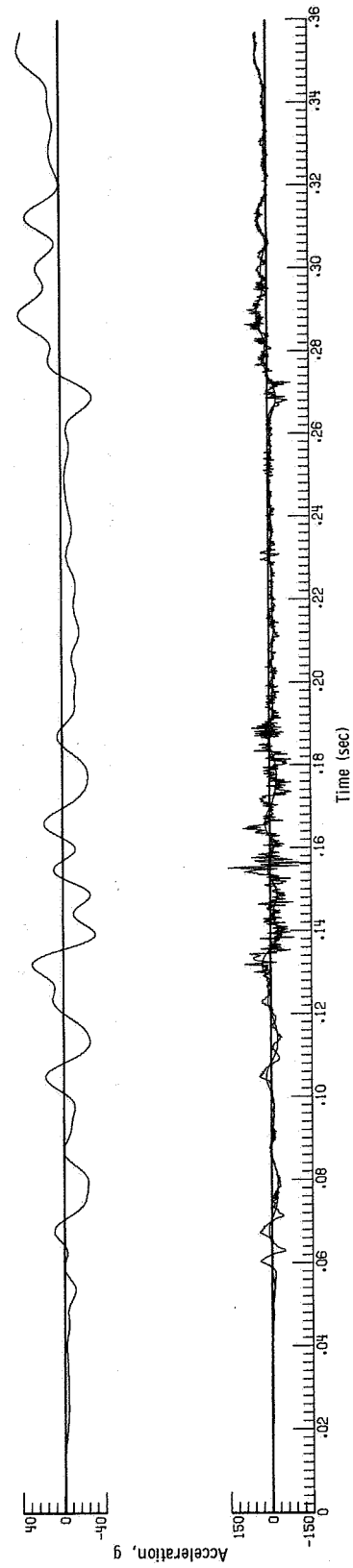


Figure 21.- Vertical accelerations for energy-absorbing crew seat.

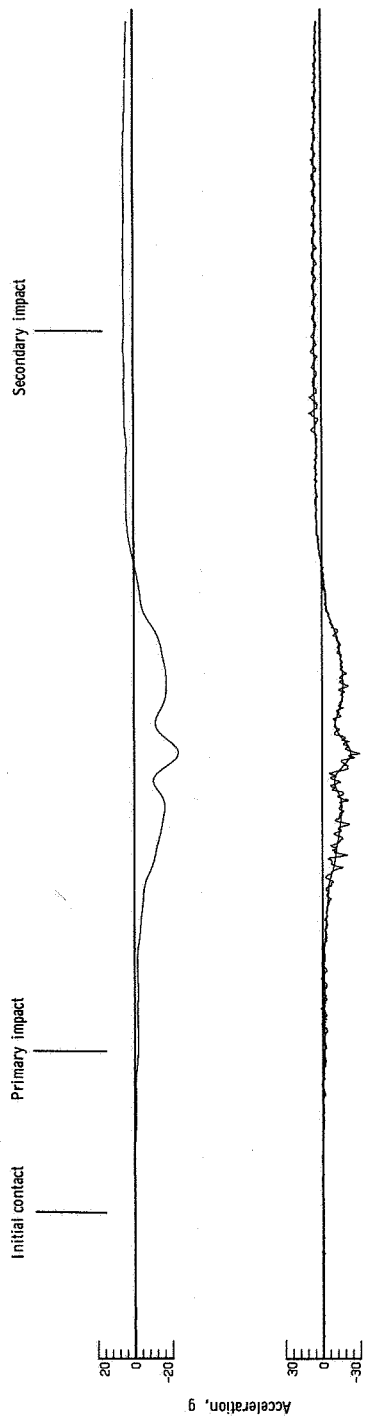


(a) Accelerometer mounted on seat back.

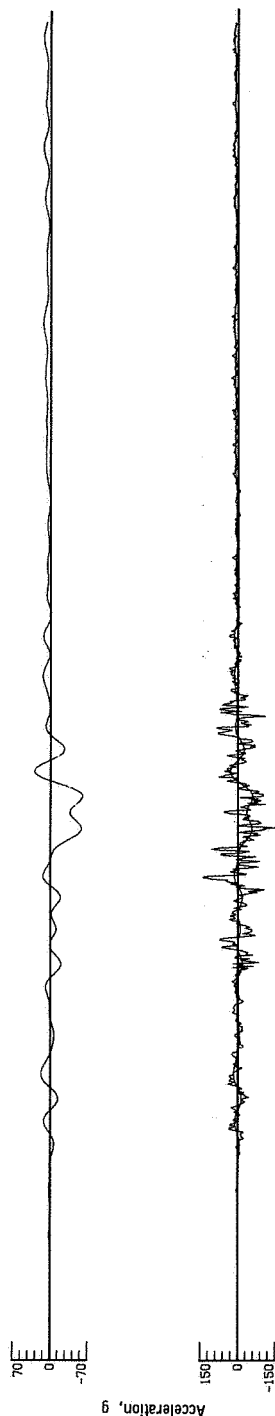


(b) Accelerometer mounted on seat floor plate.

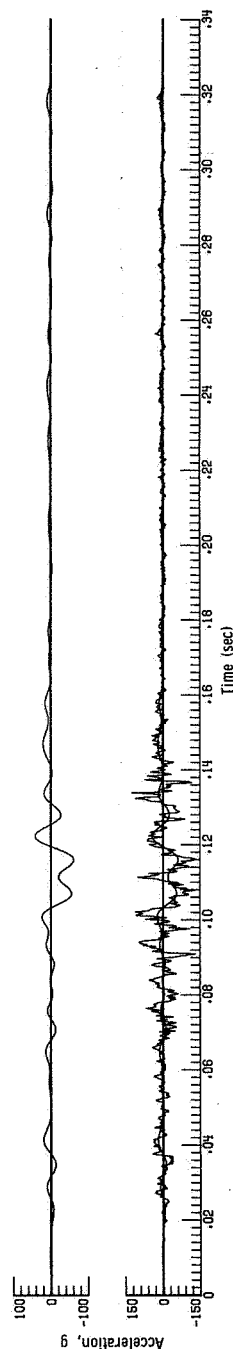
Figure 22.- Longitudinal accelerations for energy-absorbing crew seat.



(a) Accelerometer mounted in pelvic region of anthropomorphic dummy.

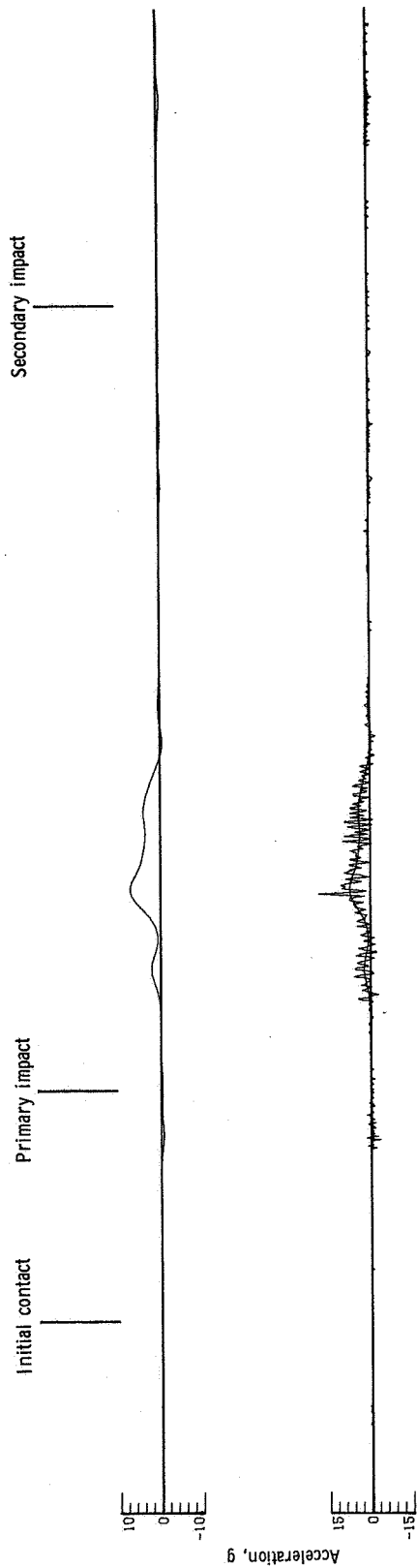


(b) Accelerometer mounted on seat floor plate center line.

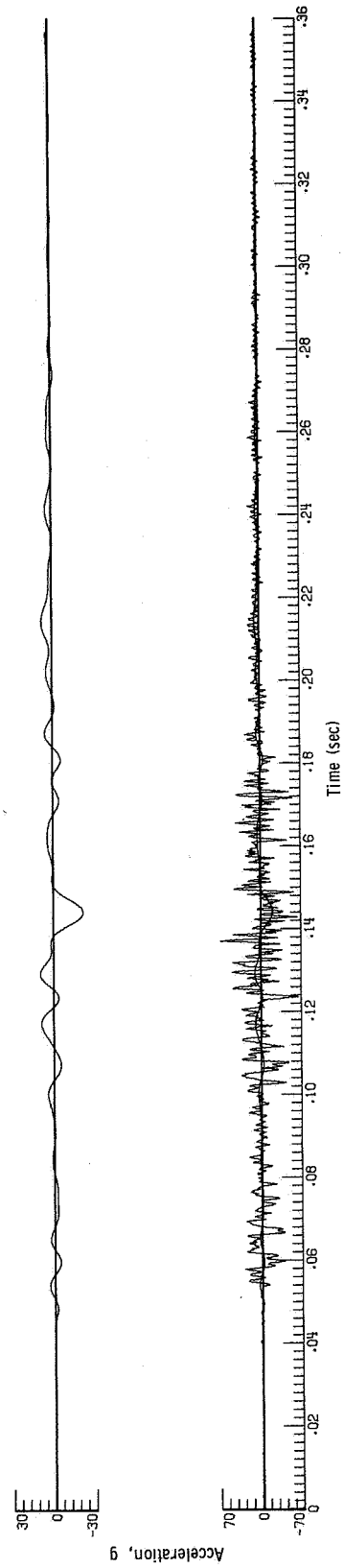


(c) Accelerometer mounted on seat floor plate off center line.

Figure 23.- Vertical accelerations for energy-absorbing troop seat.

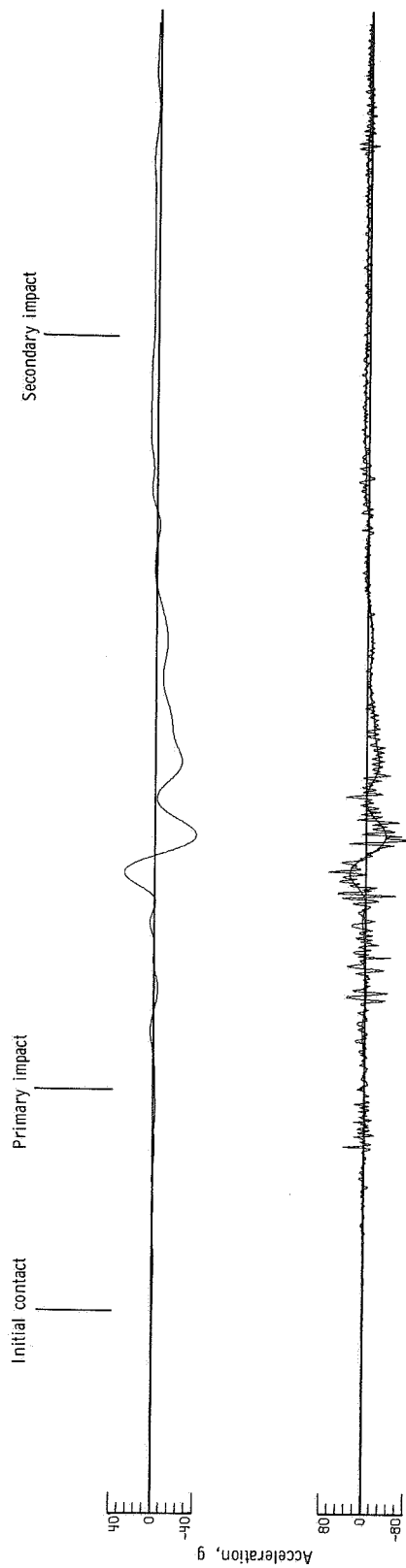


(a) Accelerometer mounted in pelvic region of anthropomorphic dummy.

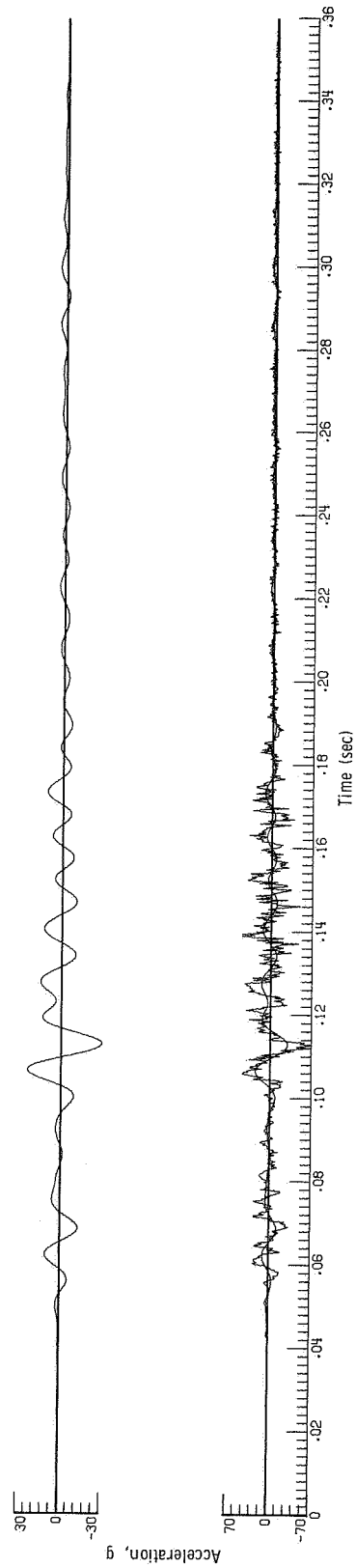


(b) Accelerometer mounted on seat floor plate.

Figure 24.- Longitudinal accelerations for energy-absorbing troop seat.



(a) Accelerometer mounted in pelvic region of anthropomorphic dummy.



(b) Accelerometer mounted on seat floor plate.

Figure 25.- Lateral accelerations for energy-absorbing troop seat.